Particle-tracking Methods for Wastewater Dispersion in Coastal Waters

Song Liu

A Thesis

In

Department

of

Building, Civil and Environmental Engineering

Presented in Partial Fulfillment of the Requirements

for the Degree of Master of Applied Science (Civil Engineering) at

Concordia University

Montreal, Quebec, Canada

April 2011

CONCORDIA UNIVERSITY

School of Graduate Studies

This is to certify that the thesis prepared

By: Song Liu

Entitled: Particle-tracking Methods for Wastewater Dispersion in Coastal Waters

and submitted in partial fulfillment of the requirements for the degree of

Master of Applied Science (Civil Engineering)

complies with the regulations of the University and meets the accepted standards with respect to originality and quality.

Signed by the final examining committee:

Dr. C. Alecsandru Chair

Dr. Z. Chen Examiner

Dr. G. Vatistas Examiner

Dr. S. Li Supervisor

Approved by Dr. M. Elektorowicz
Chair of Department or Graduate Program Director

R. A. L. Drew
Dean of Faculty

Date May 30th, 2011

ABSTRACT

Particle-tracking Methods for Wastewater Dispersion in Coastal Waters

Song Liu

This study describes the development of a particle-tracking model which predicts the trajectories of particles that apportion wastewater effluents discharged into coastal waters. The subsequent spreading of the effluents is simulated by a large number of particles evolving as clouds. The evolving cloud patterns are predicted for given time-dependent ambient currents and density stratification. The model allows for advection, non-Fickian horizontal diffusion and Richardson number-dependent vertical diffusion. The model is applied to a discharge of wastewater effluents into Burrard Inlet in British Columbia, Canada, where the ambient currents are tidally-driven and the ambient stratification results from river freshwater inflows. This application uses field measurements of ambient conditions as model input. Vertical profiles of effluent concentration derived from simulated particle distributions compare well with field measurements of effluent concentration. The model has shown advantages in handling large spatial gradients of the concentration field, and serves as a useful water-quality modelling tool.

ACKNOWLEDGEMENT

I am heartily thankful to my supervisor, Dr. Samuel Li, whose encouragement, guidance and support from the initial to the final level enabled me to develop an understanding of the subject. His perpetual energy and enthusiasm in research had motivated all his advisees, including me. In addition, he was always accessible and willing to help me, his student, with my research. As a result, research life became smooth and rewarding for me.

Lastly, I offer my gratitude and respect to my dear wife, Gina Xue, who has given me all her selfless support during the completion of the project.

Song Liu

Table of Contents

List of Figures

List of tables

List of symbols

Symbol	*Physical description*	*Unit*
C	Concentration	ppb
c_1	Constant in Eq. (3.21)	
c_2	Constant in Eq. (3.21)	
d	Total depth of channel	m
D	Horizontal diffusion coefficient	m^2/s
D_x	Diffusion coefficients on x-coordinate	m^2/s
D_y	Diffusion coefficients on y-coordinate	m^2/s
D_z	Diffusion coefficients on z-coordinate	m^2/s
g	Gravitational acceleration	m/s^2
H	Hurst index	
L	Diffuser length	m
m	Particles /Diffuser length L	m^{-1}
M	Total number of particles	
N	Brunt-Väisälä frequency	s^{-1}
Ri	Richardson number	
s	Particle settling velocity	m/s
T	Elapsed time	Sec.
t_d	Time period of particle release	Min.
u	Along-channel flow velocity	m/s
v	Cross-channel flow velocity	m/s
w	Vertical flow velocity	m/s
z_o	Near-field trapping depth	m
Δt	Integrated time interval	Min.
η	Water level	m
ξ	Random variate with zero mean and unit	
$\rho_\circ$	Reference density of seawater	kg/m^3
σ	Standard deviation	m
σ^2	Variance of particles' position	m^2
σ_0^2	Variance of particles' position at initial time	m^2

CHAPTER 1 INTRODUCTION

1.1 Specific Aims of this Study

Coastal urban centres routinely discharge municipal and industrial wastewater effluents into the near-shore water, commonly though a submarine outfall. Even if the effluents are treated to a certain level, which removes some solid and dissolved contaminants before their disposal, the remaining contaminants still enter the receiving water and subsequently spread. This will cause a water-quality problem, with adverse consequences for the creational use of the near-shore waters and for the marine ecosystem. The problem will worsen at increasing discharge rates resulting from a fast increasing urban population. Thus, it is important to understand the exposure of the receiving water to wastewater effluents from individual discharges.

Although the oceanic pollutant dispersion has attracted extensive research attention with impressive applications in many engineering designs, the understanding of the physical processes on which the models founded still remains limited. Some key hydrodynamic parameters such as diffusion coefficients and the Hurst index, which vary with ambient conditions, are almost always given assumed values. These values are very likely to be subject to significant errors. The unresolved difficulties of quantifying these parameters have prevented us from obtaining reliable solutions to the governing advection-dispersion equation. The need for an improvement has provided motivation for us to develop a reliable modelling tool for the prediction of effluent dispersion in the coastal waters.

The challenge lies in properly characterising typically rapid variations in space and time of the waste field. The rapid variations have hindered our progress in the development of modelling tools that use the Eulerian approach. In this study we aim at developing a Lagrangian numerical model for predicting the spatial and temporal evolution of effluent discharges. The model is intended for application to a tidal channel where the density is stratified.

In this study the numerical model is on the basis of random walks and simulates the trajectories of effluent particles. The model allows for both Fickian and non-Fickian diffusion. To validate the predictability of the numerical model, our strategy is to implement the modelling theory to a site for which comprehensive data are available. The general goal of this research is to advance our understanding of the effluent dispersion mechanism and to produce effective engineering solutions to control coastal pollution.

The reliable determination of relevant parameter is an important issue, which is critical to the successful prediction of effluent dispersion in the coastal waters. This issue ought to be addressed by comparing predicted waste effluent distributions with field data. For this purpose, a series of numerical experiments with a range of values for various parameters are to be conducted.

Through these numerical experiments, we wish to achieve the following specific objectives:

- Develop accurate numerical techniques for particle tracking in time- and space-dependent ambient waters.
- Determine important parameters that characterise the advection-diffusion process under tidally dominated ambient conditions.

- Quantify non-Fickian diffusion through the use of the Hurst index.
- Establish a test case with data of high quality to demonstrate the functioning and accuracy of the numerical techniques.
- Provide reasonable estimates of the parameters in the particle-tracing model for general applications to wastewater effluent dispersion in coastal waters.

1.2 Scope of the Work

To achieve the objectives outlined above, the remainder of this thesis is divided into seven chapters. Chapter 2 provides a review of the literature where background knowledge pertinent to wastewater mixing in the receiving coastal environment is summarised. An emphasis is given to the description of various models and methods developed and/or used by previous investigators for the analysis of effluent dispersion in density-stratified coastal waters.

In Chapter 3, we introduce numerical methods for particle-tracking with application to far-field calculations of wastewater effluent transport and fate. Theoretical considerations as well as detailed formulisation of particle random walks, diffusion coefficients are given. Required ambient data are also discussed.

Chapter 4 gives a detailed description of the general conditions of Burrard Inlet as an application site and of specific field surveys of the inlet. The description includes the layout of field survey zone, various types of data and field measurements of tidal currents, density stratification and dye concentrations.

Chapter 5 begins with discussion of computational procedures for particle-tracking modelling in a tidal channel. A series of model runs using the numerical techniques presented in Chapter 3 are set up to address a range of outstanding issues faced by

researchers on the topic of wastewater dispersion in the coastal environment. Details about interfacing near-field and far-field, temporal and spatial variations in the ambient conditions, discharge conditions and data comparison are given.

Chapter 6 is devoted to the presentation of numerical results for the model runs whose conditions are given in the previous chapter. The results include the general features of submerged dispersion of particle clouds. A detailed comparison of the numerical results with field measurements is given in order to confirm the predictability of the particle-tracking model. The behaviour of dispersive wastewater effluent plumes in response to ambient flows, density field and diffusion parameters, is investigated.

Chapter 7 provides a summary of the modelling methods and the application to Burrard Inlet. This is followed by conclusion drawn on the basis of comparisons between numerical results and field measurements. This research is restricted to the prediction of deterministic advective and random diffusive displacements in an idealised rectangular channel. The required input of ambient flow and density field is derived from field measurements, which is one of the limitations. This chapter ends with suggestions for future research in order to remove the limitations.

CHAPTER 2 SELECTIVE LITERATURE REVIEW

This chapter is devoted to a review of the literature on the topic of the trajectory and fate of wastewater discharges in the coastal water environment. We will first describe the physical processes that are important in the vicinity of the source (Section 2.1) and further beyond the source (Section 2.2), and then describe the advection-diffusion equation that governs the transport and mixing of effluents in the receiving environment (Section 2.3). The analytical solution to the equation in a simple case will be presented (Section 2.4). The behaviour of the solution helps us understand the difficulties in modelling of wastewater discharges using the Eulerian approach.

This chapter will be continued with the discussion of random walk techniques (Section 2.5), as a better alternative to the Eulerian approach. Then, the current knowledge of numerical modelling of the near-field mixing (Section 2.6), far-field mixing (Section 2.7), and numerical modelling of coupled near- and far-field mixing (Section 2.8) will be summarised. Next, Fickian and non-Fickian diffusion formulisations will be discussed (Section 2.9). The latter is necessary for realistic simulations. Lastly, some examples of the application of random walk techniques to coastal problems will be given (Section 2.10), before summarising this review chapter (Section 2.11).

2.1 Near-field Process

Consider the case where wastewater effluents are discharged from a treatment plant into the nearby coastal water through a submerged marine outfall. Mixing of the effluents with the receiving ambient water takes place in two distinct phases: the near field and the

(a)

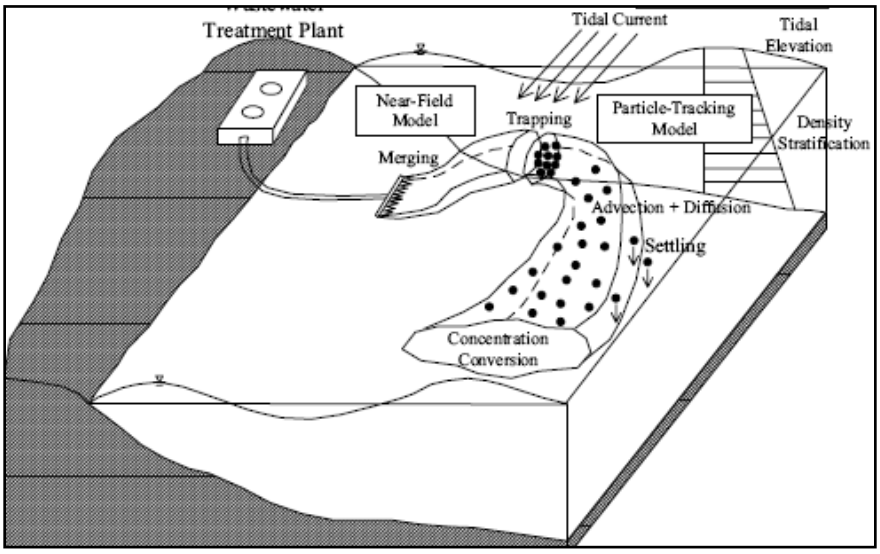

(b)

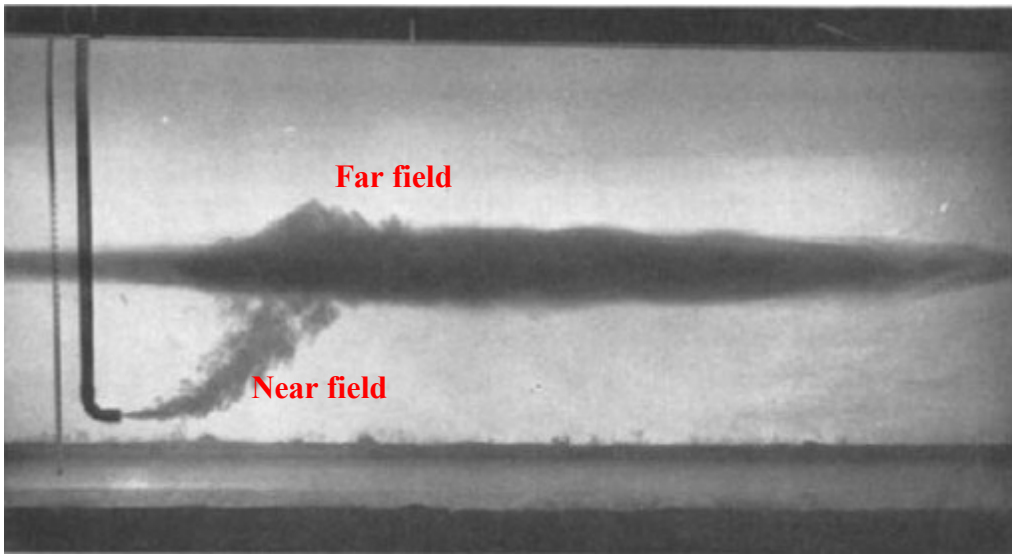

Figure 2.1 Transport and diffusion of wastewater in receiving waters: (a) a schematic diagram of marine outfall (from Kim *et al*. 2001); (b) a buoyant jet in a laboratory tank. (From Fan and Brooks 1969)

far field (Figures 2.1a,b). In the vicinity of the discharge site or the so-called near field, the initial phase of mixing is dominated by the buoyancy and momentum of discharge. In Figure 2.1b, the ambient density stratification prevents the jet from reaching the water surface.

The buoyancy is created by the difference in density between the effluents and the receiving coastal water. The former is less dense than the latter, because the effluents are typically warmer and have lower salinity than the coastal water. The effluents usually exit the outfall pipe as jet flow, and thus the discharged effluents carry initial momentum. Under the influences of buoyancy and discharge momentum, the effluents rise in the receiving water column. Meanwhile, turbulence due to buoyancy and discharge momentum entrains ambient water into the rising plumes. This near-field process ends when the diluted effluents become neutrally buoyant. The time and length scales are on the order of a few minutes and the length of the outfall (Chin & Roberts 1985).

At the end of the near-field process, the diluted effluents are trapped at a certain depth below the water surface if the receiving water is density-stratified. They may rise all the way to the water surface in un-stratified receiving water. The dilution achieved at the end of the near-field mixing is termed the initial dilution. It is desirous to achieve sub-surface trapping and maximum initial dilution.

Some of the earliest research on sewage outfalls was performed in the late 1920s by e.g. Rawn and Palmer (1930). They experimentally studied the dilution of horizontal buoyant jets in the Los Angeles Harbour. Rawn *et al*. (1961) reanalysed data from Rawn and Palmer's (1930) work using a proper hydraulic similitude; the new findings were used to optimize a multi-port outfall diffuser design. Turbulent submerged jets were

experimentally and theoretically studied by Albertson *et al*. (1950). Along similar lines, Rouse *et al*. (1952) and Scorer (1959) studied buoyant plumes. Morton *et al*. (1956) studied round buoyant plumes in a density-stratified environment. Using the entrainment assumption introduced by Morton *et al*. (1956), Brooks and Koh (1965) analytically solved, using integral-type models, the line plumes in a linearly stratified environment.

Some fundamental concepts and compressive discussion on the fluid mechanics of wastewater disposal in the ocean were given in a review paper by Koh and Brooks (1975). Gross parameter solutions of jets and plumes in various flow situations are summarized by Cederwall (1975).

2.2 Far-field Process

At further distances from the site of discharge known as the far field (Figures 2.1a,b), the ambient velocity fluctuations dominate the mixing process. At the same time, the effluent plumes are in motion due to advective transport. Models describing this phase of mixing are known as 'far-field models'. Our ability to obtain realistic solutions to the advective transport and turbulent diffusion problem is limited. This is in spite of many years of research efforts made on the topic.

2.3 Advection-diffusion Equation

The physical processes of advection and diffusion in coastal waters affect the fate and transport of pollutants in the coastal environment. As a result, the pollutant concentration C will vary in space and in time. On the basis of the principle of superposition, the two processes can be combined and the combination is mathematically expressed by the classic advection-diffusion equation

$$\frac{\partial C}{\partial t} = -\nabla \cdot (\vec{u}C) + D\nabla^2 C \tag{2.1a}$$

where t is the time, $\vec{u} = \langle u, v, w \rangle$ is the flow velocity vector field, and D is the diffusion coefficient, which can have different values in different directions.

The inverted capital Greek delta ∇ is the vector differential operator, which is defined as $\nabla = i\frac{\partial}{\partial x} + j\frac{\partial}{\partial y} + k\frac{\partial}{\partial z}$, where i, j, k is the unit vector in the x-, y-, and z-direction.

In Equation (2.1a, b), it has been assumed that the advection and diffusion processes are linearly independent, which is convenient and advantageous from the computational point of view. It has also assumed an incompressible fluid for which the equation of continuity is given by $\nabla \cdot \vec{u} = 0$. In three dimensions, Equation (2.1a) may be rewritten as

$$\frac{\partial C}{\partial t} + \frac{\partial}{\partial x}(uC) + \frac{\partial}{\partial y}(vC) + \frac{\partial}{\partial z}(wC) = D_x \frac{\partial^2 C}{\partial x^2} + D_y \frac{\partial^2 C}{\partial y^2} + D_z \frac{\partial^2 C}{\partial z^2} \tag{2.1b}$$

where D_x, D_y and D_z are the turbulent diffusion coefficients in the x-, y- and z-directions, respectively.

It is important to note that molecular diffusion is not significant for mixing of pollutants in the coastal environment, compared to mixing caused by turbulent diffusion. Accordingly, in Equation (2.1a), the term on the left hand side represents the time rate of change of the concentration C in a control volume (Figure 2.2); on the right hand side, $\vec{u}C$ in the first term represents the advective mass flux per unit area per unit time, and $D\nabla C$ in the second term represents the net diffusive mass flux due to turbulent fluctuations.

This diffusive mass flux has been formulated using the analogy of turbulent mixing to random molecular diffusion. The traditional formulation of molecular diffusion is based on the Fick's law that states that the diffusive flux of materials is proportional to the concentration gradient and the proportional coefficient D is constant. However, the mixing process associated with turbulence in natural water bodies is non-Fickian, meaning that the use of constant values for the coefficient is not adequate.

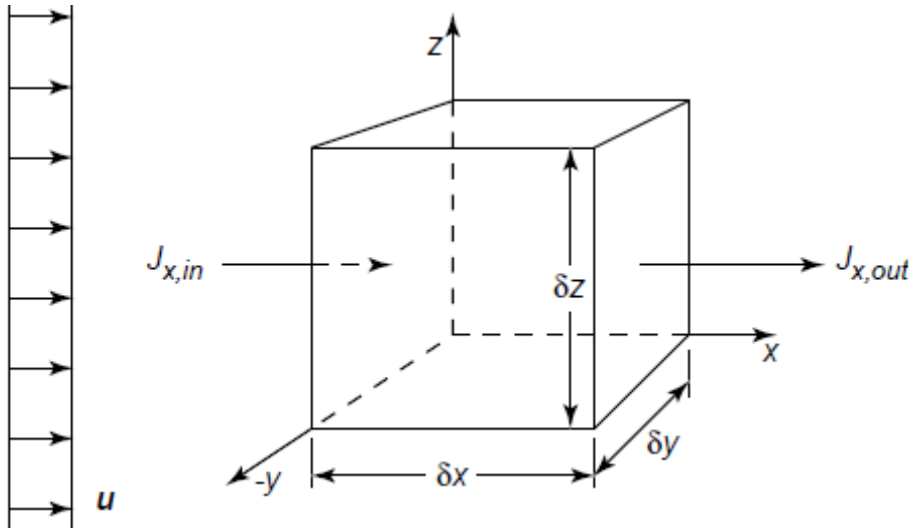

Figure 2.2 A schematic control volume with cross flow. The dimensions are δx, δy and δz. J_x is the mass flux into or out from the control volume (from Socolofsky and Jirka 2005).

2.4 Point-source Solution

Analytical solutions to Equation (2.1) can only be obtained in very limited simple cases. For example, if the problem is one-dimensional (say in the x-direction) and the velocity u is constant, one may simplify the problem by introducing a moving coordinate system. The new independent variables are: $\eta = (x - x_\circ + ut)$ and $\tau = t$, where x_o is the location of a point source of tracer, ut is the distance traveled by the center of mass of the

cloud in time *t*. Using the chain rule for differentiation, it can be shown that Equation (2.1) is reduced to

$$\frac{\partial C}{\partial \tau} = D_x \frac{\partial^2 C}{\partial \eta^2} \tag{2.2}$$

For an instantaneous point source, Equation (2.2) has an analytical solution, given by

$$C(\eta,\tau) = \frac{M}{A\sqrt{4\pi D_x \tau}} \exp\left(-\frac{\eta^2}{4D_x\tau}\right) \tag{2.3}$$

where $A = \delta y \delta z$ and $M = C\delta x \delta y \delta z$. In the physical domain, the behaviour of this solution for three different times t_1, t_2, and t_3, is shown in Figure 2.3. On one hand, the initial concentration 'spike' at $\tau = 0$ is seen to spread out in time. On the other hand, there is a significant spatial gradient on both sides of the spike at any given time. At the very large times, concentrations asymptotically approach zero for all η.

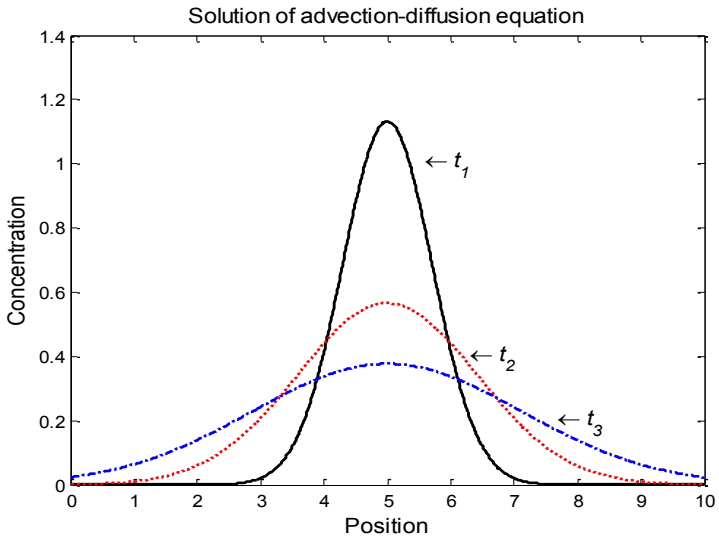

Figure 2.3 Schematic solution of the advection-diffusion equation in one dimension. The dotted line plots the maximum concentration as the cloud moves downstream from the right to the left (from Socolofsky and Jirka 2005)

The graph shown in Figure 2.3 describes the diffusion of a large pulse of contaminant into a thin tube of fluid, which can be considered as one-dimensional. In the coastal environment, the velocity field is typically three-dimensional and time-dependent. The turbulent diffusion coefficient changes with time and space. Moreover, the model domain often contains irregular shorelines and uneven bottom topography. These complex factors make it extremely difficult if not impossible to obtain analytical solutions to the advection-diffusion equation. Numerical approaches represent a good alternative. There are two major types of numerical approaches: the Eulerian and Lagrangian approaches. Random walk techniques fall into the Lagrangian category.

2.5 Random Walk Techniques

In a flow field with velocity fluctuations the trajectory of a particle may be thought of as resulting from successive random displacements, superimposed to the advective, deterministic displacements. A random walk is a mathematical description of the trajectory. In random walk techniques, the released pollutant mass is represented by a large number of discrete particles; computations commence from time t equal to zero, and at each time step, each particle follows a "random walk". The underlying assumption is that there is no correlation between the random walk directions of two consecutive time steps.

Random walk techniques have been shown as a reliable tool for producing numerical solutions to the advection-diffusion equation (2.1b), as discussed in a review paper by Barry (1990). The techniques have found useful applications in pollutant

transport problems. The temporal and spatial distributions of the pollutant concentration field may be derived from random walk simulations.

Since the 1950s, random walk techniques have been applied in the analysis of diffusion and dispersion of contaminants in groundwater (Scheidegger 1954; De Jong 1958; Prickett *et al*. 1981). Some random walk models are limited to one-dimension (e.g. Hathhorn 1997) and the others consider two-horizontal dimensions (Kinzelbach 1988) in their predictions of the movement of polluted particles in groundwater. The basic concepts of the techniques for groundwater applications can be found in e.g. Kinzelbach (1986).

Within the context of groundwater modelling, Valocchi and Quinodoz (1989) successfully used the techniques to simulate the one-dimensional transport of kinetically adsorbing solutes. Adsorption is directly incorporated into the particle tracking algorithm by utilizing an analytical formula for the probability density function of the fraction of time a particle spends in the aqueous phase. Although the numerical results showed a good agreement with the analytical solutions, the relative error in the variance estimation is sensitive to the reaction rates as well as the number of particles used. Therefore, it would be important to conduct sensitivity tests with respect to the total of particles released to the flow field.

Banton *et al*. (1997) proposed a method described as the time domain random walk method to simulate the solute transport in one-dimensional heterogeneous media. The model calculates the arrival time of a particle cloud at a given location. In a homogeneous zone, the breakthrough curve can be calculated directly at a given distance using a few

hundred particles or directly at the boundary of the zone. The authors emphasize the importance of an extension to three dimensions.

In atmospheric applications, random walk techniques have successfully been used to study coastal fumigation phenomena (Luhar and Sawford 1995) and buoyant dispersion in convective boundary layer (Luhar and Britter 1992).

Random walk models have been used to study pollutant transport and dispersion in surface waters by a number of researchers. Examples include the study of pollutant transport in natural rivers by Jeng and Holley (1986) and the investigation of thermal pollution in rivers by Pearce *et al*. (1990). Random walk models have also be applied to the problem of pollutant discharges in coastal waters (Scott 1997; Chin and Roberts 1985; Kim and Seo 2001). Scott (1997) considered the problem of pollutant discharges in tidal waters and solved the advection-diffusion equation using particle tracking techniques in two horizontal dimensions. The stochastic solutions were shown to be in reasonable agreement with an analytical solution due to Kay (1987), but the formulisation is invalid for submerged plume simulations because it ignores vertical variations.

However, there are a good deal of issues still outstanding. Firstly, the vertical dimension is missing, as most of the existing random walk simulations have considered two or even one horizontal dimension. Second, density stratification tends to suppress velocity fluctuations in the vertical, which has important implications for random walks in the vertical, but is typically ignored. Third, there are only a limited number of coastal discharge applications, as revealed by a search of the literature.

To produce the desired dispersive effects in contaminant transport modelling, random steps of the Gaussian distribution are commonly used. Although the distribution

has the advantages of possessing a quantifiable mean and variance, and at the same time satisfying the condition of probabilistic continuity, Gaussian distributed random steps take long computational time to generate. According to Hathhorn (1997), Gaussian distributed random steps are not necessary. Alternatively, uniformly distributed steps, which are computationally efficient, can be employed as long as a few basic statistical requirements are met. For instance, it is required to exclude the possibility of large displacements occurring within the incremental stepping time.

2.6 Near-Field Modelling

Detailed analysis of the near-field process and related calculations has been extensively studied in the past 50 years. Brooks (1956) studied the performance of ocean outfall diffusers and made an application to an outfall from a small digested sludge treatment plant. Later, the author analytically solved the surface dilution of the wastes (Brooks 1960). Impressive contributions were made by Roberts, Snyer and Baumgartner in 1989. About 100 experiments were conducted in which different combinations of diffuser port spacing, jet velocity, effluent density, and current speed and direction were studied. The key findings from these experiments are as follows:

- The effluent plume's rise height and thickness decrease as the current speed increases.
- Dilution increases with current speed for all current directions, with diffusers perpendicular to the current resulting in higher dilutions than when parallel.
- Dilution shows no dependency on port spacing or source momentum flux over the parameter range tested and the dominant source parameter is the buoyancy flux per unit length.

- The initial mixing region where the buoyancy-induced turbulence is actively entraining ambient fluid and diluting the effluent is confined primarily to the rising plumes for zero current speed, but can be swept far downstream for flowing currents.
- Within the mixing region the layer thickness and dilution increase. The dilution due to initial mixing reaches a limiting value at some distance from the diffuser and then remains constant.

Jirka and Doneker (1991) suggested a hydrodynamic-flow-classification scheme that applies to the near-field behaviour of submerged single-port discharges. In their view, two flow patterns stand at the opposite extremes of the whole spectrum of near-field flow behaviour: a small, gently rising buoyant jet in deep water as one extreme, and a strong, violently mixing discharge flow exhibiting instabilities and recirculation over the entire water depth as the other. Many other flow patterns will exist between these two extremes. The scheme based on various length scales, ambient currents and geometric variables, classifies the possible flow configurations into 35 flow categories.

Following the above-mentioned concepts, Jirka and Akar (1991) extended the classification to the submerged multiport configurations in arbitrary ambient conditions by defining 32 generic flow classes in three major categories: internally trapped flow in linear ambient stratification, buoyant flows in uniform ambient layers, and negatively buoyant flows in uniform ambient layers. This classification methodology provides a good guide to analyst in the choice of predictive models and serves as a helper in screening all the possible flows.

2.7 Far-Field Modelling

Two different approaches, namely the Eulerian and Lagrangian formulisations, have been used in order to simulate the far-field mixing process expressed mathematically by Equation (2.1). The traditional Eulerian approach is very efficient when applied to a smooth flow field. However, it may give large errors when the velocity field undergoes significant variations in both magnitude and direction. Consequently, this drawback limits its applications when dealing with large concentration gradients in space. It is not unusual that the Eulerian approach produces unphysical results of negative concentrations and suffers from purely numerical diffusion.

The above-mentioned problems associated with the Eulerian approach can be avoided by using the Lagrangian approach. In this approach, the effluent mass is apportioned into a large number of particles. At any given time, the trajectories of all the particles are predicted. The Lagrangian approach ensures mass conservation and non-negative concentrations, without difficulties. It is free of numerical diffusion.

Bensabat *et al*. (2000) developed an adaptive pathline-based particle tracking algorithm. The purpose is to improve the accuracy in the evaluation of the Lagrangian concentration in the Eulerian-Lagrangian method for the solution of advection-dispersion problems. The algorithm involves splitting the travel time (in a transport simulation time step) into a set of smaller travel time increments so that the linear approximation of mean tracking velocity produces accurate tracking in a quasi uniform flow within each increment. In this way, a high accuracy is obtained, since exact tracking can be achieved for a uniform flow field. The accuracy of particle tracking is improved by refining the particle tracking process along element boundaries on an inter-element basis and by

subdividing the travel time along the particle's path into a number of travel time increments. The proposed algorithm improves the efficiency of particle tracking by locally subdividing the tracking process in regions where the velocity varies significantly into more tracking steps than in regions with smooth variations in the velocity.

2.8 Hybrid Modelling Combined with Near-Field and Far-Field

Much of the early work has treated the near-field and far-field separately. This treatment may suffer a discontinuity problem at the interface between two fields. The reason is far-field model cannot resolve the near-field mixing and near-field model usually ignores various ambient conditions which dominate the far-field effluent diffusion.

Kim and Seo (2001) proposed a 3-D hybrid model which combined near and far field. The initial mixing in the near field is modelled using line plume equations suggested by Roberts *et al*. (1989). The advection and dispersion in the far field are simulated using the random-walk particle-tracking model. The velocity field of the ambient water is calculated by a three-dimensional hydrodynamic model. The length, width, height and thickness of wastefield obtained from the near-field model are then fed into far-field transport model as the initial condition values. When applied to an outfall discharge in Masan-Jinhae Bay in Korea, the model appears to yield results in reasonable agreement with field data through calibration. However, the model is based on Fickian diffusion. This is a significant shortcoming, which would limit the general use of the model, in particular when the ambient conditions are strongly time-dependent.

Li and Hodgins (2004) developed a hybrid model that combines near- and far-field processes, for the study of the dilution and dispersion behaviour of effluents discharged

into a tidal channel. Near-field computations from a U.S. EPA line buoyant plume model (UM), provide an estimation of cross-sectional average (across plume) effluent dilution between the diffuser ports and the point of effluent plume trapping. The near-field computations also provide the corresponding plume element velocity, plume trapping depth and centreline trajectory. Far-field computations are based on the equation of continuity and momentum balance in three dimensions, together with the advection-diffusion equation. The main findings are as follows: In the near-field the dilution behaviour and plume trapping in tidal waters are controlled by the tidal currents and are more sensitive to effluent discharge rate than to ambient stratification; an increase in the effluent flow rate produces shallower trapping and reduced initial dilution. The hybrid model uses the Eulerian approach, which is known to encounter difficulties in capturing large spatial gradients.

2.9 Fickian and Non-Fickian Dispersion

The traditional particle-tracking techniques employ random Brownian motion to simulate turbulent dispersion. Particle dispersions are assumed to be homogeneous in the horizontal. In other words, a particle executes a simple random walk, without preference in its direction from step to step and without dependence on the size of particle clouds. Field observations (e.g. Osborne *et al*. 1989; Sanderson and Booth 1991), however, strongly indicate that particle dispersions increase over the time. To address this issue Hurst (1951) introduced a Hurst index H in the evaluation of the dispersion coefficient. H appears as a scaling exponent of the elapsed time. If $H = 0.5$, the dispersion is Fickian. If $H > 0.5$, the dispersion is non-Fickian.

Osborne *et al*. (1989) and Sanderson and Booth (1991) studied non-Fickian dispersion processes and found that the trajectories of satellite-tracked ocean surface drifters may be described as persistent fractional Brownian motions with non-Fickian scaling properties. Their studies dealt with two separate regions of the globe: the Northeast Atlantic and the Kurisho extension, but yielded a general agreement that the Hurst index is all around 0.79 with an error of 0.07.

Similar results were reported in Addison *et al.* (1997). They simulated surface diffusion in an idealized open bay and compared Fickian and non-Fickian formulisations. A Hurst exponent of 0.75 was employed in both *x*- and *y*-directions. Relative to Fickian dispersion, non-Fickian dispersion observed a noticeable increase in the spreading rate of the particle cloud over the time. In physical terms, this would mean a sharper reduction in contaminant concentration. However, Addison *et al*.'s (1997) predictions have not been validated using experimental or field data. Perceivably, in reality, complex topography of receiving water and different density of drifters or particles would lead to different values for the Hurst index.

The above-mentioned investigations have ignored vertical variations in the ambient conditions. However, it is understood from the investigations that one should consider non-Fickian horizontal dispersion so as to produce realistic results of particle dispersions in coastal waters with varying flow and density stratification.

2.10 Applications of Particle Tracking Techniques

Particle-tracking techniques have been applied in studies of many coastal water problems. Chin and Roberts (1985) used the techniques in their simulations of the far field dispersion of wastewater instantaneously and continuously discharged from ocean

outfalls. They predicted the temporal and spatial variations of maximum concentration, diffusing cloud size, and diffusion coefficient. Their work has led to the development of some semi-empirical equations for the determination of the maximum concentration and the variance of the concentration distribution.

Particle tracking method also found its application in sedimentary system. In a study of sand-recycling and sand-bypassing behaviour, Tajima *et al*. (2007) developed a numerical model which tracks certain groups of sand grains deposited on the sea bed. The model yields such predictions as volume of total sand grains in motion, mean movement of sand grains, and the dispersive characteristic of the group of dumped sand grains. In the calculation of random walk, the combined effects of wave and currents were considered. The dispersion coefficient was adjusted to obtain model results that are consistent with experimental data.

2.11 Summary

Numerous liquid waste of municipal, industrial and agricultural sources is discharged into the nearby water bodies. Different dispersion patterns may take place as the effluents mix with the ambient water. Mixing occurs in two phases: near-field mixing and far-field mixing, with different control factors. The near-field process is influence by the dynamic and thermal characteristics of the discharge, notably the momentum and buoyancy fluxes, and by the outfall geometry and ambient conditions in the vicinity of the discharge. Further beyond the immediate near-field is the far-field region where the discharge characteristics are no longer important. The conditions of the ambient environment dictate the trajectory and fate of the effluents through the process of

advection and oceanic turbulent mixing. Passive diffusion caused by the ambient turbulence is important (Jirka and Doneker 1991).

There are two approaches to the simulation of far field mixing: the Eulerian approach and the Lagrangian approach. Numerically, the Eulerian approach gives concentration solutions to the advection-diffusion equation in fixed positions. The main drawback of Eulerian numerical solutions is related to the large distortion in the area of significant variations in concentration. The Lagrangian numerical techniques, specifically Monte Carlo methods, have been suggested to be the most useful techniques in the study of turbulent diffusion (Chin and Roberts 1985).

Most of particle-tracking simulations have employed a Fickian dispersion model (with the Hurst index H = 0.5) to simulate turbulent mixing in the far-field. However, field observations have evidenced that effluent motions in coastal waters are persistent fractional Brownian motions with non-Fickian scaling properties. That is to say that H is larger than 0.5 (Addison *et al*. 1997). In reality, quantifying H in the coastal zone can be complex (List *et al*. 1990). Some researchers have suggested that H is around 0.79 (Osborne *et al*. 1989, Sanderson *et al.* 1991). Others suggested that $H \approx 0.75$ (Addison *et al*. 1997). However, all these suggested H values have not taken into account vertical variations of the ambient conditions.

Horizontal dispersion in coastal waters is not well understood despite of earlier researchers' efforts made to tackle the problem. Field observations suggest that the horizontal dispersion coefficient ranges from 0.01 to 13 m^2/s (Steven *et al*. 2004). In some instances the dispersion rate increases more rapidly than expected based on empirical generalizations from the ocean and smaller lakes. The theory of dispersion in

ocean or lakes at short times is not sufficiently well developed, especially when concerned with the interaction of internal waves, currents and the geometry conditions. To specify the expected values of mixing parameters further study is required.

CHAPTER 3 PARTICLE-TRACKING MODEL

3.1 Introduction

The purpose of this chapter is to present the computational methods for the spreading of wastewater effluents in the coastal water environment. We first discuss the Lagrangian Method (Section 3.2) that is suitable for particle tracking, and then move on to describe the initial distributions of particles (Section 3.3). The mean ambient flow field in which motions of the particles take place may be obtained in a number of ways (Section 3.4). Since in reality the ambient flow field contains turbulent fluctuations, we further discuss the process of random walks in three-dimensions (Section 3.5), which allows for the influence of the turbulent fluctuations on the trajectory traced by an effluent particle as it travels in the ambient water.

In the coastal water, turbulent fluctuations in the ambient flow field are typically larger in the horizontal than in the vertical. The consideration of such a distinction is important for the mathematical formulisation of random walks. We use the analogy of random walks caused by turbulent eddies to diffusion models, and consider non-Fickian diffusion models in the horizontal (Section 3.6) and in the vertical (Section 3.7). In the formulation of the vertical diffusion coefficient, we take into account the competing effects of velocity shear and density stratification.

3.2 The Lagrangian Method

When studying the transport and dispersion of pollutants in coastal waters, we wish to track individual effluent particles' motion. The Lagrangian method is a method of

description that follows a particle (see e.g. Fox *et al*. 2004), which is particularly useful for our study. As illustrated in Figure 3.1, the particle moves in an ambient velocity field. At time *t*, the particle is at the position (x, y, z) in the Cartesian coordinates; the associated position vector is $\vec{r}$. At this position, the particle immediately assumes a velocity corresponding to the ambient velocity $\vec{v}(x, y, z, t)$ at that point in three-dimensional space at time *t*.

At time $t + \Delta t$ where Δt is a small time increment, the particle has moved to a new position $(x + \Delta x, y + \Delta y, z + \Delta z)$; the corresponding position vector is $\vec{r} + \Delta\vec{r}$ (Figure 3.1). The particle instantly has a velocity given by $\vec{v}(x + \Delta x, y + \Delta y, z + \Delta z, t + \Delta t)$. Between time *t* and time $t + \Delta t$, we may write

$$x(t + \Delta t) = x(t) + u(\vec{r}, t)\Delta t \tag{3.1}$$

$$y(t + \Delta t) = y(t) + v(\vec{r}, t)\Delta t \tag{3.2}$$

$$z(t + \Delta t) = z(t) + [w(\vec{r}, t) + s]\Delta t \tag{3.3}$$

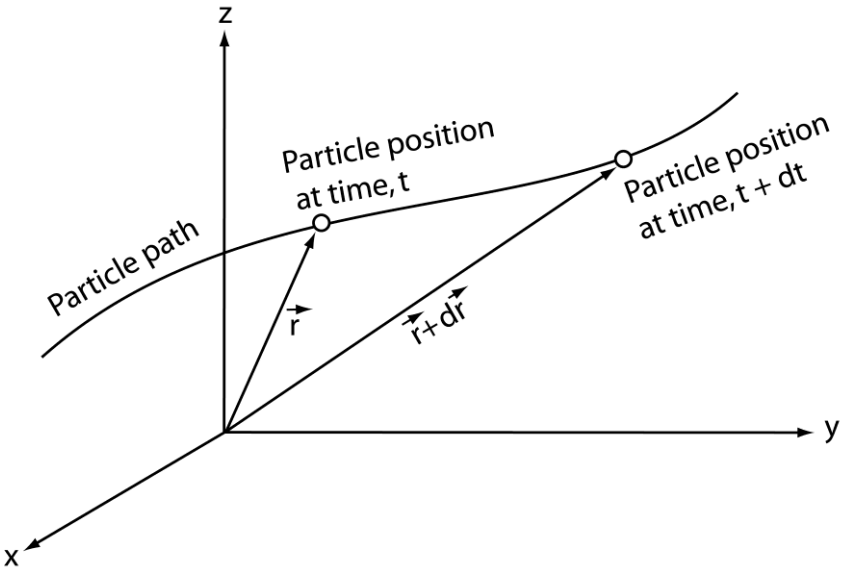

Figure 3.1 Motion of an effluent particle in a flow field.

where s is the particle-settling velocity; u, v, and w are the ambient velocity components of the ambient flow field. The consideration of particle settling is more important if the focus is on long-term impact of a discharge on the receiving water quality. The velocity components in Equations (3.1)–(3.3) are evaluated at the position $\vec{r} = \langle x, y, z \rangle$ at time t. The advective displacements in the x-, y- and z-direction, $u\Delta t$, $v\Delta t$, $w\Delta t$ are deterministic. It is important to note that in coastal waters, ambient velocities typically vary in both space and time and so are the displacements.

Equations (3.1)–(3.3) are to be applied to a large number of particles. In addition to the condition of the ambient flow field, the possible trajectories of the particles depend on their initial positions. One is not free to choose the initial positions, because they are the result of the so-called near-field process.

3.3 Initial Distributions of Particles

The effluent mass discharged either spontaneously or continuously into the receiving water is apportioned into a total of M particles (Figure 3.2). In the case of a spontaneous discharge, the cloud of M particles enters the receiving water at the same initial time $t = 0$. For convenience, let this initial time correspond to the end of the near-field process, where the key control parameters include discharge momentum, buoyancy force and configurations of diffuser ports (Roberts *et al*. 1989a,b; Jirka and Doneker 1991; Li and Hodgins 2004).

It is assumed that at time $t = 0$, the M particles are evenly distributed over the diffuser's length L in the y-direction (Figure 3.2), i.e. there are

$$m = \begin{cases} M/L, & n = 1 \\ 0, & n > 1 \end{cases} \tag{3.4}$$

particles per-unit-length of diffuser, where n = 1, 2, ..., N, denotes the number of time steps of a particle-tracking simulation. The even distribution of particles in the y-direction implies that the subsequent motions of the released particles should show statistically the same dispersion patterns at any vertical planes that are parallel to the xz coordinates plane and within the diffuser's length L.

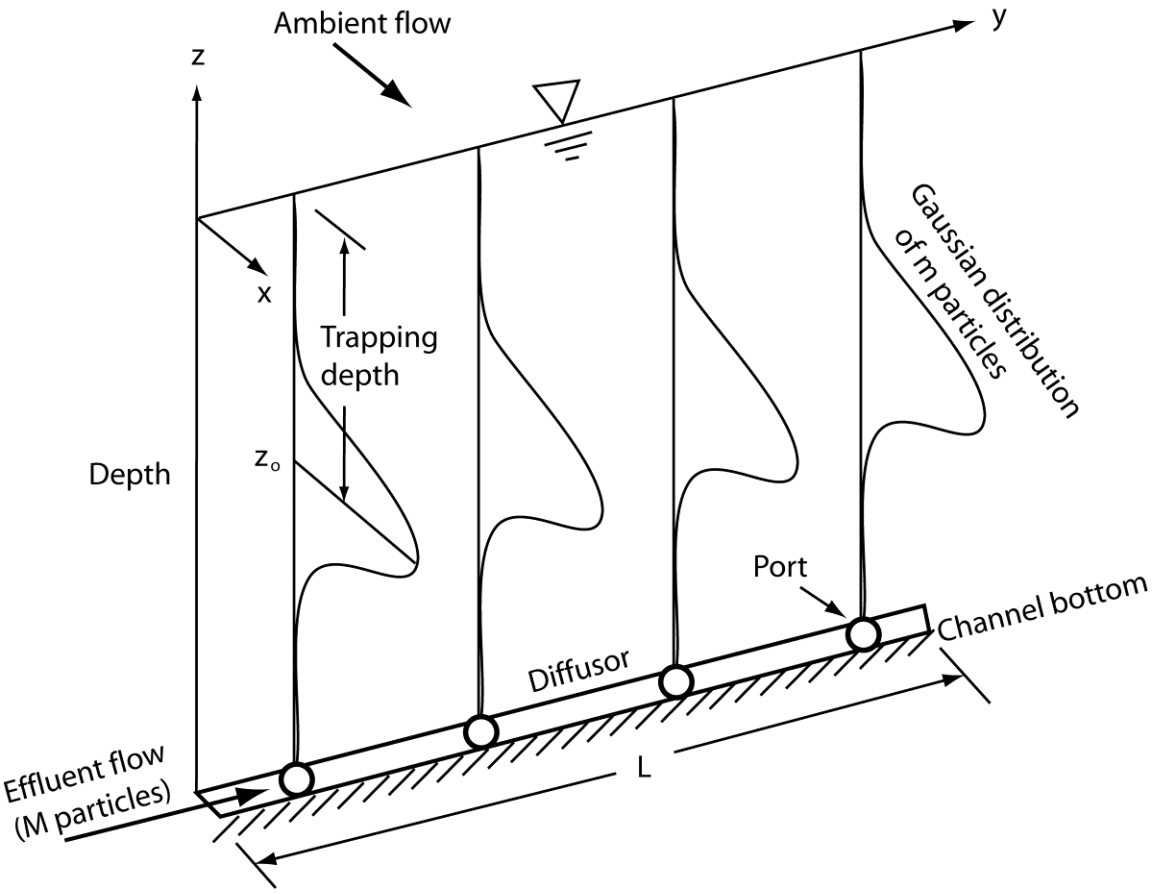

Figure 3.2 Initial distributions of effluent particles for a particle-tracking simulation. Wastewater effluents emerge from a series of diffuser ports and rise rapidly in the water column under the influence of discharge momentum and buoyancy in the near field. At the end (denoted by time t = 0) of the near-field process, the particles may be trapped within a narrow range of depth.

In the case of continuous discharge, a total of M particles are released into the receiving water over a prescribed period of time t_d. Thus, the number of particles released in one time step Δt is $M\Delta t/t_d$. In the like manner as the case of spontaneous discharge, the $M\Delta t/t_d$ particles are evenly distributed over the diffuser's length (Figure 3.2). The number of particles per-unit-length of diffuser in one time step is

$$m = \begin{cases} M\Delta t/(t_d L), & n \le t_d/\Delta t \\ 0, & n > t_d/\Delta t \end{cases} \tag{3.5}$$

In the vertical, the m particles are assumed to follow the Gaussian distribution. The associated probability density function p is given

$$p(z) = \frac{1}{\sqrt{2\pi\sigma^2}} e^{-\frac{(z-z_o)^2}{2\sigma^2}} \tag{3.6}$$

where z_o is the location of the peak of the distribution, and σ^2 is the variance. z_o is located at the so-called plume trapping depth (Figure 3.2). This trapping depth as well as the variance will be derived from field measurements, which will be discussed later. The function p given in Equation (3.6) satisfies the following condition

$$\int_0^d p(z)dz = m \tag{3.7}$$

where d is the total depth of flow. In general, a Gaussian distribution is valid for effluent concentration at the end of near-field mixing for diffuser discharges, as evidenced in experimental data (Lee & Chu, 2003) and in field measurements of effluent concentration made from the vicinity of the source (Li & Hodgins, 2010).

At the time they enter the receiving water from the diffuser, all the particles have x-coordinates of zero. Subsequently or at time $t = 2\Delta t, 3\Delta t, ..., N\Delta t$ of a simulation, the

motions of those particles that have entered the receiving water are tracked. The total time covered by the simulation is *T*.

3.4 Ambient Flow Field

As input to particle-tracking modelling, the ambient flow field of a given model domain may be obtained in a number of ways: e.g. numerical hydrodynamics simulations, harmonic predictions and field surveys. If all the hydrodynamic forcing of importance as well as the detailed geometry of the model domain, with good accuracy, are known, the spatially and temporally varying flow field can be predicted using a hydrodynamics model. There are many successful examples for application to the transport and dispersion of effluents from outfall discharges (see e.g. Kim and Seo 2001; Li and Hodgins 2004, 2010). However, the use of hydrodynamics models for flow predictions is limited to the situation where field data are available for verification of the predictions.

If the needed ambient flow is driven mainly by the tides, classic harmonic analysis would be the most useful technique for prediction of the tidally-driven ambient flow. Details of the technique can be found in Godin (1972). Using harmonic constants of tidal constituents that are significant for the model region, the technique can provide predictions of tidal flow for any required duration of time in any time interval. In Table 3.1, an example of tidal flow predictions is shown for Burrard Inlet (Station ID: 7795 Point Atkinson, B.C.; location: 49°20'N, 123°15') on the coast of British Columbia. For this station, the significant tidal constituents include semidiurnal tidal constituents M2, S2 and N2, and diurnal tidal constituents K1, O1 and P1.

One may also derive the ambient flow field from measurements of water velocities made from a coastal area of interest. If available, field measurements of velocities may be a preferable source of data particularly for the purpose of verifying a newly developed model. The use of ambient flow velocities based on field measurements avoids the issue of uncertainties in hydrodynamic or harmonic predictions. The field measurements used in this study will be discussed in the next chapter.

Table 3.1 Predicted tidal currents in Burrard Inlet (First Narrows) for January 2004. The flood (+) direction is 135° true north. The ebb (-) direction is 315° true north. (Data source: NOAA, U.S.A.)

Day	Slack Water Time h.m.	Max. Current		Slack Water Time h.m.	Max. Current		Slack Water Time h.m.	Max. Current		Slack Water Time h.m.	Max. Current		Slack Wate Time h.m.
		Time h.m.	Velocity knots		Time h.m.	Velocity knots		Time h.m.	Velocity knots		Time h.m.	Velocity knots	
1	225	435	-0.9	640	1010	2	1300	1705	-3.7	2100			
2		10	2.5	405	555	-0.7	750	1100	1.5	1330	1745	-3.9	2135
3		100	3.1	510	705	-0.8	915	1150	1.1	1355	1825	-4.1	2210
4		145	3.6	600	805	-1	1030	1235	0.8	1420	1900	-4.2	2245
5		220	4.1	640	850	-1.2	1135	1320	0.6	1450	1940	-4.3	2320
6		300	4.4	715	930	-1.4	1230	1400	0.5	1525	2015	-4.4	2355
7		335	4.6	750	1010	-1.5	1310	1440	0.5	1605	2050	-4.5	
8	30	410	4.7	820	1045	-1.6	1340	1520	0.6	1650	2130	-4.5	
9	105	440	4.7	850	1115	-1.7	1415	1600	0.7	1735	2205	-4.5	
10	140	515	407	920	1150	-1.9	1450	1640	0.9	1825	2245	-4.3	
11	215	550	4.5	945	1220	-2.1	1530	1730	1	1920	2325	-3.9	
12	250	625	4.3	1010	1300	-2.4	1615	1820	1.1	2025			
13		15	-3.3	330	700	3.9	1035	1340	-2.8	1710	1925	1.3	2140
14		105	-2.6	410	740	3.4	1100	1425	-3.3	1805	2040	1.6	2320
15		215	-1.8	455	825	2.8	1130	1515	-3.7	1905	2200	2.2	
16	120	335	-1.1	550	915	2.2	1205	1605	-4.2	2000	1315	2.9	

All times listed are in Local Time, and all speeds are in knots.

(From http://co-ops.nos.noaa.gov/currents04/BURRARDI.shtml, accessed on March 13, 2011)

3.5 Random Walk

The kinematic formulisation given in Equations (3.1)–(3.3) is deterministic, without considering turbulent fluctuations in the ambient flow. These fluctuations inevitably cause chaotic motions of particles and thus must be taken into account. It is not feasible to explicitly resolve the turbulent fluctuations in particle-tracking modelling, but their effects can be incorporated by superposing random walks (x', y', z') to the formulisation. Thus, the motion of an effluent particle is described by

$$x(t+\Delta t) = x(t) + u(\vec{r}, t)\Delta t + x'(t) \tag{3.8}$$

$$y(t+\Delta t) = y(t) + v(\vec{r}, t)\Delta t + y'(t) \tag{3.9}$$

$$z(t+\Delta t) = z(t) + w(\vec{r}, t)\Delta t + z'(t) \tag{3.10}$$

The second term on the right hand side of the above equations represents the displacement of a particle due to advection. The particle-settling velocity in Equation (3.3) has been dropped as our focus is on short-time simulations, for which particle-settling is less important. As a result of advection and random walk, a particle may arrive at one of many possible positions at a new time step, as illustrated in Figure 3.3 on the *xy*-plane.

Consider the random walks in the *x*-direction of up to *M* particles at time *t* $X' = \{x'_1, x'_2, \cdots, x'_i, \cdots, x'_{M-1}, x'_M\}$, where the subscript *i* is used for the *i*'th particle. The variance of the X' distribution is defined by

$$\sigma_{X'}{}^2 = E[(X' - E[X'])^2] \tag{3.11}$$

where $E[X']$ stands for the statistical expectation of X'. Equation (3.11) represents the mean of the square of the deviation of X' from its mean level $E[X']$.

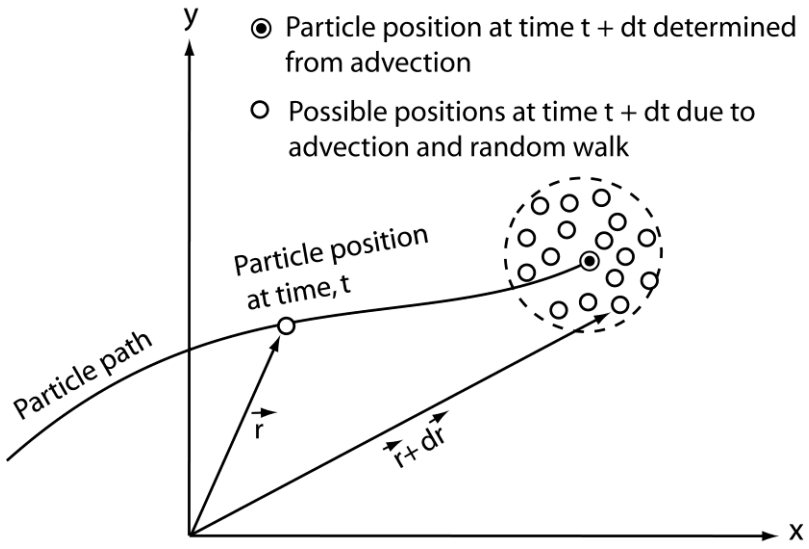

Figure 3.3 Motion of a particle in a flow field due to advection and random walk.

Two criteria are used to generate the random walks $\{x'_1, x'_2, \cdots, x'_i, \cdots, x'_{M-1}, x'_M\}$. The first criterion is that the statistical expectation is zero, i.e.

$$E[X'] = 0 \tag{3.12}$$

The second criterion concerns the variance of X'. Because of the first criterion given in Equation (3.12), the variance in Equation (3.11) is simplified to

$$\sigma_{X'}{}^2 = E[(X')^2] \tag{3.13}$$

The diffusion coefficient, D_x, may be defined as the time rate of increase of the variance $\sigma_{X'}{}^2$ or $D_x = \frac{1}{2}\frac{d}{dt}\left(\sigma_{X'}{}^2\right)$. Equation (3.13) can be rewritten as $E[(X')^2] = \frac{d}{dt}\left(\sigma_{X'}{}^2\right)\Delta t$ or

$$E[(X')^2] = 2D_x \Delta t \tag{3.14}$$

It can be shown that the two criteria given by Equations (3.12) and (3.14) are satisfied by the random walk process of the form

$$X' = \xi\sqrt{2D_x \Delta t} \tag{3.15}$$

where ξ is an independent, normally distributed random variate with zero mean and unit variance. Values for ξ are obtained by sampling from ξ = -0.5 to 0.5.

We assume simple symmetric random walks in the horizontal, i.e. an effluent particle having the same probabilities of walk jumping in any direction (Figure 3.3). By following the procedures for generating random walks in the *x*-direction, one may obtain the y-direction random walks as below

$$Y' = \xi\sqrt{2D_y \Delta t} \tag{3.16}$$

The diffusion coefficients D_x and D_y for random walks in the *x*- and *y*-direction [Equations (3.15) and (3.16)], will be calculated using non-Fickian formulisation.

3.6 Horizontal Diffusion Coefficient

For simple symmetric random walks in the horizontal, the two diffusion coefficients, D_x and D_y, should have the same value at any given time. Non-Fickian diffusion means that the coefficients are time-dependent. At time t = 0, the coefficients have an initial value, which may be defined as $D_x = D_y = \sigma_\circ^2 / \Delta t$, where σ_o^2 is the variance of the distribution of up to M particles at the end of the near-field process. At subsequent times $t > 0$, the variance of the dispersing particle cloud can be expressed as

$$\sigma^2 = (\sigma_\circ^2 / \Delta t) t^{2H} \tag{3.17}$$

where H is the Hurst index (Hurst 1951). Correspondingly, the diffusion coefficients are evaluated as the derivative of the variance with respect to time. In other words, they are given by

$$D_x = D_y = 2H(\sigma_\circ^2 / \Delta t) t^{2H-1} \tag{3.18}$$

When the Hurst index is given a value larger than 0.5, the variance of the dispersing particle cloud increases non-linearly with time. The diffusion becomes non-Fickian, and the diffusion coefficients are time-dependent. In the special case of H = 0.5, the values for D_x and D_y do not increase with time, and hence the diffusion process recovers the Fickian condition.

3.7 Vertical Diffusion Coefficient

In the vertical, turbulent fluctuations of the ambient flow field and the resultant mixing are related to velocity shear in the vertical and ambient density stratification. Therefore, these two factors affect random walks in the vertical. We relate the random walks to vertical diffusion as

$$Z' = \xi\sqrt{2D_z\Delta t} \tag{3.19}$$

where D_z is the vertical diffusion coefficient. This coefficient is calculated using a Richardson number-dependent formula. The Richardson number is defined as

$$Ri = \frac{N^2}{\left(\partial u/\partial z\right)^2 + \left(\partial v/\partial z\right)^2} \tag{3.20}$$

where $N \equiv \sqrt{-\frac{g}{\rho_\circ}\frac{\partial \rho}{\partial z}}$ is the Brunt-Väisälä frequency, g is the gravitational acceleration, ρ is the density of ambient water varying with depth, and $\rho_\circ$ is the reference density of ambient water (or seawater density under normal condition) The Richardson number measures the relative importance of velocity shear and gravitationally stable density stratification. The former tends to intensify turbulence, whereas the latter inhibits turbulence. D_z is related to the Richardson number as

$$D_z = \frac{c_1\sqrt{(\partial u/\partial z)^2 + (\partial v/\partial z)^2}}{1 + c_2 Ri}(d - z)z \tag{3.21}$$

where c_1 and c_2 are constants, and d is the total depth of ambient water. The above expression yields zero D_z on the free surface ($z = 0$) and the seabed ($z = d$). A minimum value of $1.0\text{x}10^{-4}$ m^2/s is given to D_z.

Because of the spatial variations in D_z, it is necessary to modify Equation (3.10) for an individual particle. The modification follows the suggestion of Kinzelbach and Uffink (1991), given by

$$z(t + \Delta t) = z(t) + [w(\vec{r}(t), t) + \partial D_z / \partial z]\Delta t + \sqrt{2D_z \Delta t}\,\xi \tag{3.22}$$

The added term involves the derivative of the vertical diffusion coefficient $\partial D_z / \partial z$, evaluated at the current location $\vec{r}(t)$ at time t. This addition represents an adjustment to the advective velocity. It ensures that the results of particle-tracking modelling correspond to solutions to the advection-diffusion equation [Equation (2.1b)].

CHAPTER 4 APPLICATION

4.1 Background

The particle-tracking modelling techniques presented in Chapter 3 can potentially be applied to many water bodies that receive discharges of wastewater effluents from land-based wastewater treatment plants. In Table 4.1, some marine outfalls in Canada are listed. These outfalls are part of important infrastructures that service the public and the industrial sector that discharges effluents into the nearby coastal water. However, the discharges potentially pose adverse impacts on the receiving water quality and jeopardise the creational use of the receiving water.

This chapter deals with an application of the modelling techniques to Burrard Inlet on the British Columbia coast (Figure 4.1), which has been receiving wastewater effluents from the Lions Gate Wastewater Treatment Plant (Figure 4.2). This plant provides primary treatment to wastewater originating from West Vancouver and the City and District of North Vancouver. The plant is located immediately to the west of Lions Gate Bridge in West Vancouver (Figure 4.2) and discharges effluents into the inlet at First Narrows through an outfall equipped with a diffuser.

The general conditions of ambient flow and stratification of the inlet are described in Section 4.2. Section 4.3 gives an outline of a comprehensive field survey conducted in the inlet as a source of input and validation data for modelling the Lions Gate discharge. Field measurements of effluent plumes and ambient conditions in coastal waters are difficult and expensive to make. Thus, the field survey represents a valuable source of data for this study.

Table 4.1 A summary of marine outfalls in Canada

Outfall name & province	Service population (thousand people)	Daily Discharge Capacity (1MLD=1000m3/s)	Receiving water
Lions Gates, Vancouver, B.C.	174	92.4 (2006)	English Bay
Lulu Island, Vancouver, B.C.	120	80 MLD (2006)	Fraser River mouth
Ashbridge Bay, Toronto, ON	1524	818 MLD (2009)	Lake Ontaria
Bonnybrook, Calgary, AB	600	376 MLD (2008)	Bow River
Quebec City, QC	1225	676.8 MLD (2010)	St. Lawrence River

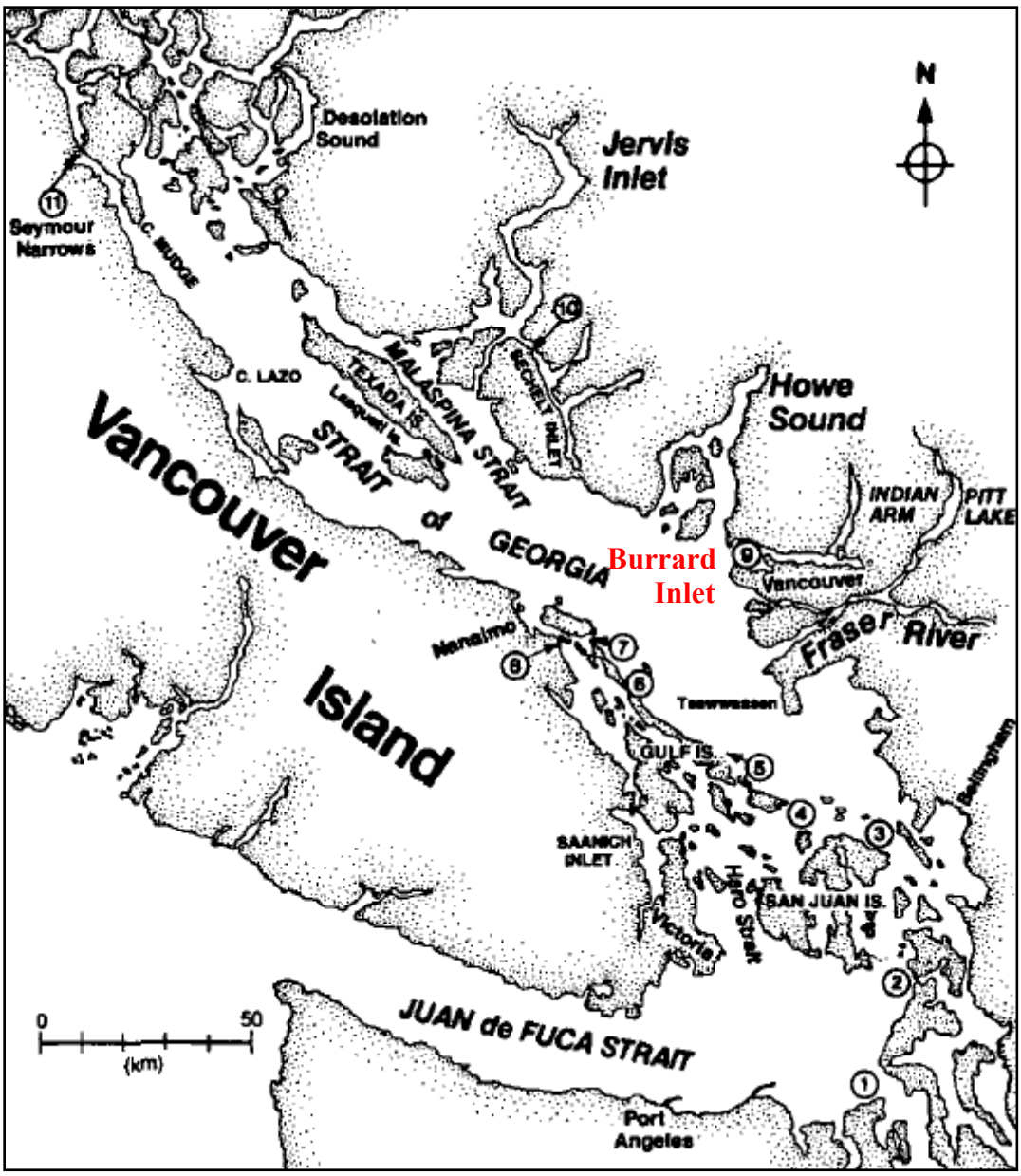

Figure 4.1 Map of the southern B. C. coast, showing the Strait of Georgia (Thomson 1981).

4.2 General Ambient Conditions of Burrard Inlet

Thomson (1981) gave a description of the oceanography of the B.C. Coast, including Burrard Inlet. The inlet features mixed diurnal-semidiurnal tides. Diurnal and semi-diurnal tides refer to the rhythmic rise and fall of sea level one and two cycles per lunar day, respectively. The tides on the B.C. coast are purely diurnal or semidiurnal for only a few days each month. Most of the time, they are mixed diurnal and semidiurnal tides. The tides in Burrard Inlet are classified as mixed, predominantly semidiurnal.

Tidal waves propagate from the Pacific Ocean into the Strait of Georgia through Juan de Fuca Strait (Figure 4.1). The associated tidal flows affect Burrard Inlet (circled number 9 in Figure 4.1), which is the site of application in this study.

The flow patterns in Burrard Inlet, as illustrated in Figures 4.3a-d, are associated with tidal flows featuring back-and-forth motions. The figures show the surface flow patterns on large flood, small flood, large ebb and small ebb. During large flood and ebb tides the flow speeds range from 25 to 50 cm/s, whereas during small flood and ebb the flow speeds are about 25 cm/s, except in First Narrows where the flow speeds generally exceed 50 cm/s. The flow patterns illustrated in Figures 4.3a-d should be viewed as general representations of the actual flow at various stages of the tides.

On a large flood, the northward flows in the Strait of Georgia (Figure 4.1a) turn into the inlet (north-easterly currents) in the vicinity of Point Grey (Fig 4.3a). An accompanying south-easterly flow enters the inlet off Point Atkinson. Over most of the inlet, the surface flows are then directed toward First Narrows, and attain maximum speeds of around 25-50 cm/s. Due to funnelling, the flood flows through First Narrows

reach 3 m/s during spring tides. During small floods, the flow pattern is similar to that of a large flood except that mid-channel flows are weaker and tend to broaden more within the inlet (Fig. 4.3b). More pronounced northerly flows appear at the strait entrance to the inlet, and the counter clockwise eddy to the left of Point Atkinson extends westward.

On a large ebb the surface flow (Figure 4.3c) shows a pronounced feature that the strong, narrow currents extend from First Narrows to Point Atkinson. The core of the flow at such times is offshore and has the maximum velocities of around 100 cm/s. During small ebbs, the north-shore jet is weaker and less well established so the counter clockwise eddy that appears on large ebbs (Figure 4.3c) does not form over the eastern portion of the inlet (Figure 4.3d). However, ebb flows still tend to be directed northward along the beaches of Stanley Park.

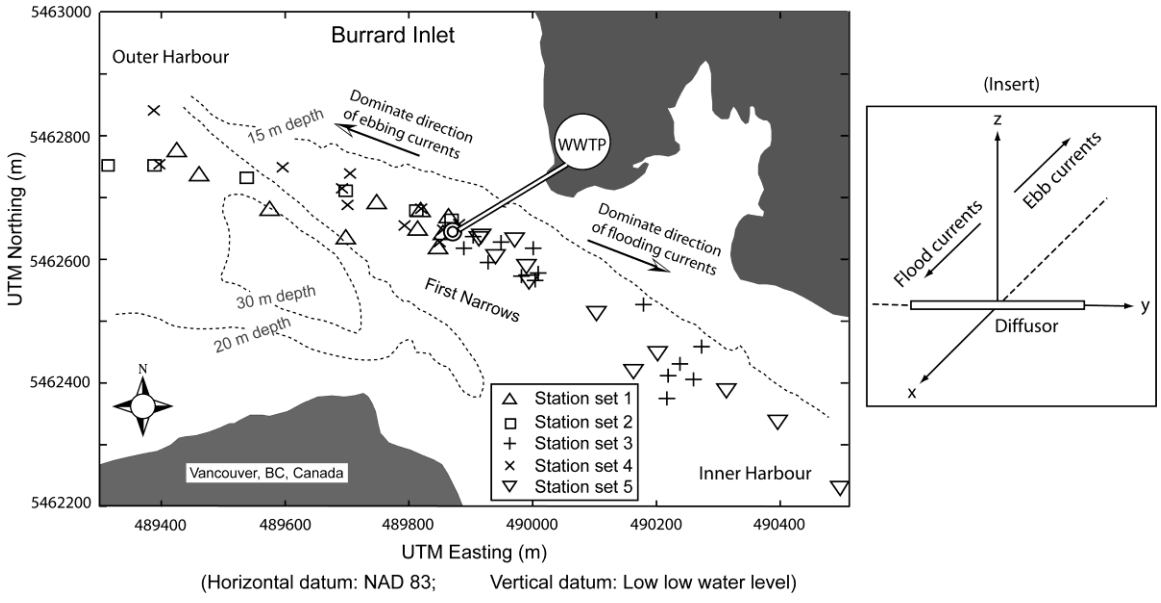

Figure 4.2 Map of the discharge site, showing the channel geometry, the directions of ebbing and flooding currents and survey stations. The insert panel shows the Cartesian Coordinates system used for particle tracking (Modified from Li & Hodgins, 2010).

(a)

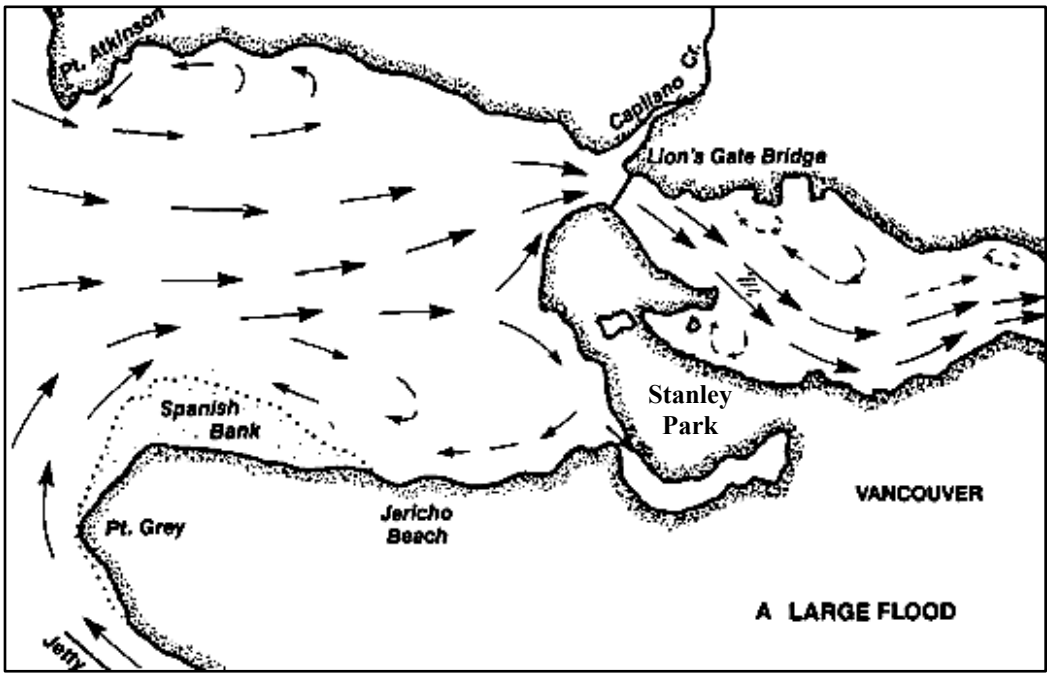
Pt. Atkinson
Capilano Cr.
Lion's Gate Bridge
Stanley Park
Spanish Bank
Pt. Grey
Jericho Beach
VANCOUVER
A LARGE FLOOD

(b)

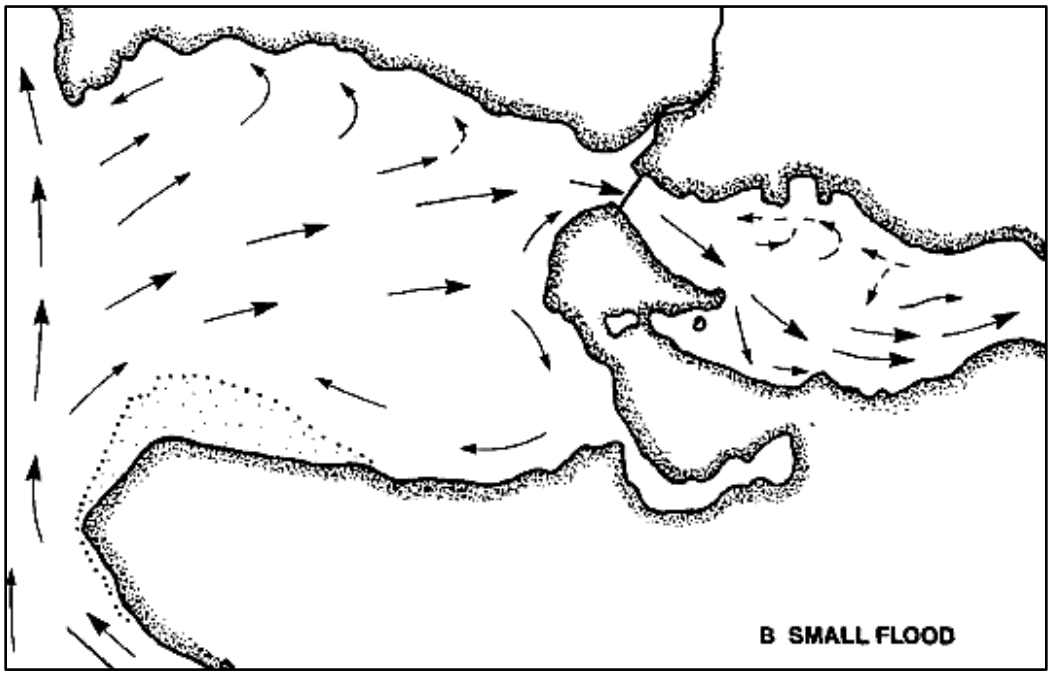
B SMALL FLOOD

(c)

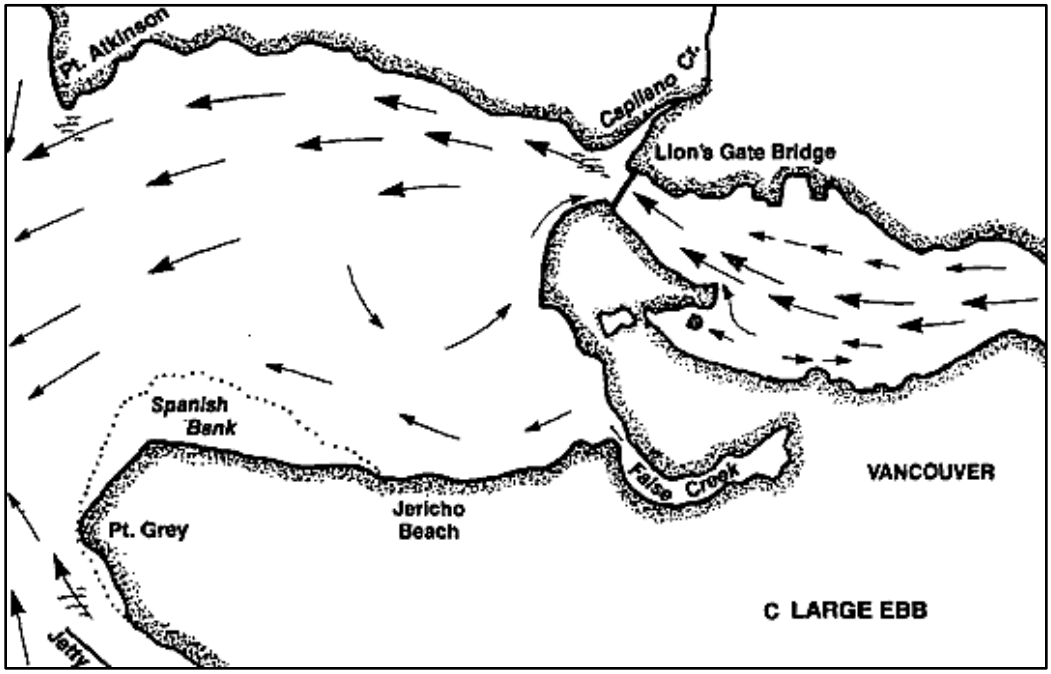
Pt. Atkinson
Capilano Ct.
Lion's Gate Bridge
Spanish Bank
False Creek
VANCOUVER
Jericho Beach
Pt. Grey
C LARGE EBB

(d)

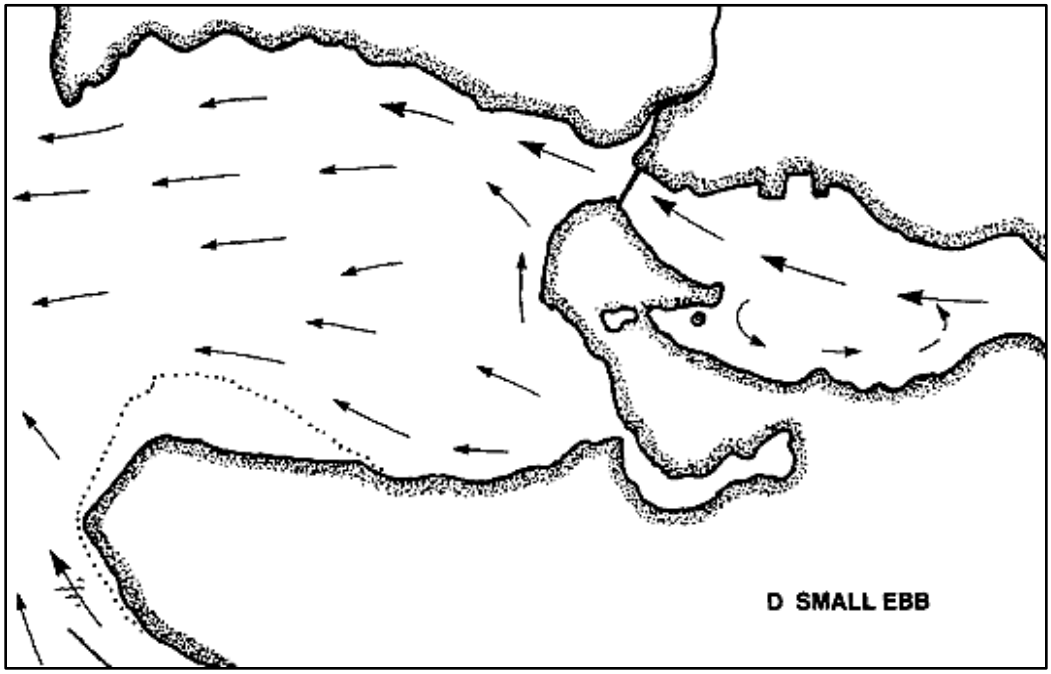
D SMALL EBB

Figure 4.3 Tidal currents in Burrard Inlet: (a) large flood, (b) small flood, (c) large ebb, and (d) small ebb. (Adapted from Campbell 1954)

The general conditions of flow patterns and density stratification have important implications for the dispersion and trapping of wastewater plumes in the inlet. However, the ambient conditions that are qualitatively described above are insufficient for the purpose of detailed modelling of wastewater effluent dispersion. In the following, we will discuss field measurements of high quality used in this study.

4.3 Field Surveys

Particle-tracking modelling of the Lions Gate discharge uses input data mostly derived from dye-tracing surveys conducted in Burrard Inlet in September 1998 (Seaconsult 1999). Survey stations and area coverage are shown in Figure 4.3. During the time periods of the surveys, Rhodamine dye liquid was added to the effluents in the wastewater treatment plant (WWTP). Concentrations of dye in the effluents were measured in the plant using a fluorometer (a device used to measure parameters of fluorescence). The effluent flow rates varying throughout the survey periods were also measured in the plant. The dyed effluents entered the inlet in First Narrows through an outfall pipe.

In addition to the measurements made in the plant, the surveys in the inlet water provided field measurements of

- exposure zones of wastewater effluents within English Bay and Inner Harbour of the inlet,
- vertical profiles of effluent concentrations in the inlet water,

- ambient flow velocities in the vicinity of First Narrows, and
- ambient density stratification in the inlet.

Details of data processing, field methods and instrument accuracy can be found in Seaconsult (1999). For completeness, we provide a summary below.

4.3.1 Diffuser and Effluent Flowrate

The outfall is located just to the west of the Lions Gate Bridge and runs along a trench cut into the seabed at the narrowest point in the First Narrows channel. A 10-port diffuser is fitted to the end of the outfall, located between 184 and 227 m from shore. The average water depth over the diffuser is about 20 m below mean sea level. The present effluent flow rates range from 0.9 m^3/s to 2.4 m^3/s, with an average dry weather flow rate of 1.0 m^3/s. The peak wet weather flow capacity is 3.3 m^3/s. Future upgrades to the plant will increase its capacity to 4.0 m^3/s.

4.3.2 Current Profile

Vertical profiles of water velocities were measured at a station about 150 m west of the diffuser using a 300 kHz Acoustic Doppler Current Profiler (ADCP) mounted in a trawl-resistant bottom stand. The instrument was deployed on September 16, 1998 and recovered on September 29, 1998.

The data were processed to provide a vertical profile of current speed and direction every 15 minutes with a resolution of 0.5 m between 3.55 m above the bottom and surface. Data were not obtained at the seabed since the design of an acoustic Doppler current meter results in some data loss immediately above the sensors. There is also some

data loss at the surface, amounting to about 10% of water depth (2m), produced by the acoustic beam orientation of 20° off-vertical.

From the measurements three velocity profiles can be obtained at distinct tidal phases: peak flooding tide, peak ebbing tide and slack water. For all other tidal phases, velocity profiles can be obtained by linear interpolations of the three velocity profiles.

4.3.3 Density Profile

Vertical profiles of water temperature, salinity and depth were made in the field using a Sea Bird SBE19 conductivity-temperature-depth instrument (CTD) during the period of dye injections. The density of water is derived from the measurements of temperature, salinity and depth. In addition, these density profiles were verified using historic measurements from the area, which have been considered as the reference. These historic data were obtained over the period of 1975 - 1995 in various research projects. The accuracy of the density values is good for the purpose of the present study although the vertical resolution varies from relatively poor in 1975 to good in 1995 as a result of instrumentation improvement.

4.3.4 Effluent Concentrations

Two dye injections were carried out on September 26, 1998, each lasting for approximately 3 hours. The starting times corresponded to slack water in order to cover the entire tidal phase of flooding or ebbing. Since one of the concerns is related to effluent exposure during periods of minimum dilution, small tides were selected for the periods of dye injection. This selection also facilitated accurate measurements of dye

concentrations because tidal currents through First Narrows were at their lowest making vessel handling and instrument control much less difficult than during larger spring tides.

The dye injections were timed for determining minimum dilution in the initial dilution zone during slack water, followed by tracing the dispersion pathway and dilution of effluent into Outer Harbour or the Inner Harbour depending on the tide phase.

Dye concentration data were acquired with a fluorometer, operated in both towed and vertical profiling modes. The instrument package consists of a Variosens in situ fluorometer and a CTD connected to the DATAQ automated data acquisition system. The Variosens fluorometer was calibrated prior to the field survey using a sample of the raw dye stock supplied for this project, and yielded the calibration curve for the future measurements. The Rhodamine concentration (ppb) unit, which related to the Variosens voltage measurement, was introduced to calibrate vertical dye concentration profiles, the spatial extent of effluent discharge, as well as locating the point of minimum dilution.

The dye concentration data were sampled at one-half second intervals and automatically logged to hard disk files for computer processing. Each profile has an associated position whose coordinate origin located at the mid-point of outfall (5462645N 489871E). North American datum 1983 is used for all position data in this study.

Data processing for the vertical profiles consisted of quality controlling the calibrated data, synchronizing the position data with profile and then separating the down-cast and up-cast portions of each profile. Since there was some unavoidable boat movement during the profile measurement, the down-casts and up-cast were generally

separated by a few metres and represent nearly-independent profiles of the plume structure. For more details, refer to Seaconsult (1999).

CHAPTER 5 NUMERICAL SIMULATIONS

5.1 Computational Procedures and Model Parameters

Mathlab code has been developed for the implementation of the particle-tracking methods described in Chapter 3 and for result visualisation. A conceptual flow chart is shown in Figure 5.1. Computations commence from the specification of model parameters, importation of ambient flow velocity profiles and importation of ambient density profiles. In a simulation, some model parameters are given constant values, whereas the others depend on time or space or both, as summarised in Table 5.1. The Hurst index H is an important parameter ranging from 0.5 and 0.7. A higher value for the index means that the rate of spreading of particle clouds increases with elapsed time.

Computations proceed to derive ambient conditions of flow velocity and density from the field observations described in Sections 4.3.2 and 4.3.3. The derived velocity field and density field are spatially distributed and cover all time steps over the time period of a simulation.

Computations then move on to giving initial positions of all the particles. Without losing generality, their x-coordinates are taken as zero and their y-coordinates are such that the particles are evenly distributed along the length of a diffuser (Figure 3.2). Their z-coordinates are assumed to follow the Gaussian distribution; the probability density function is given in Eq. (3.6). The shape of the function (Figure 5.2) depends on the location of the peak or z_o in Figure 3.2 and the variance σ^2. We choose $\sigma^2 = 1$ and z_o = 12 m, because the corresponding vertical profile matches dye-concentration profiles observed in the vicinity of the source from the field survey described in Section 4.3.4.

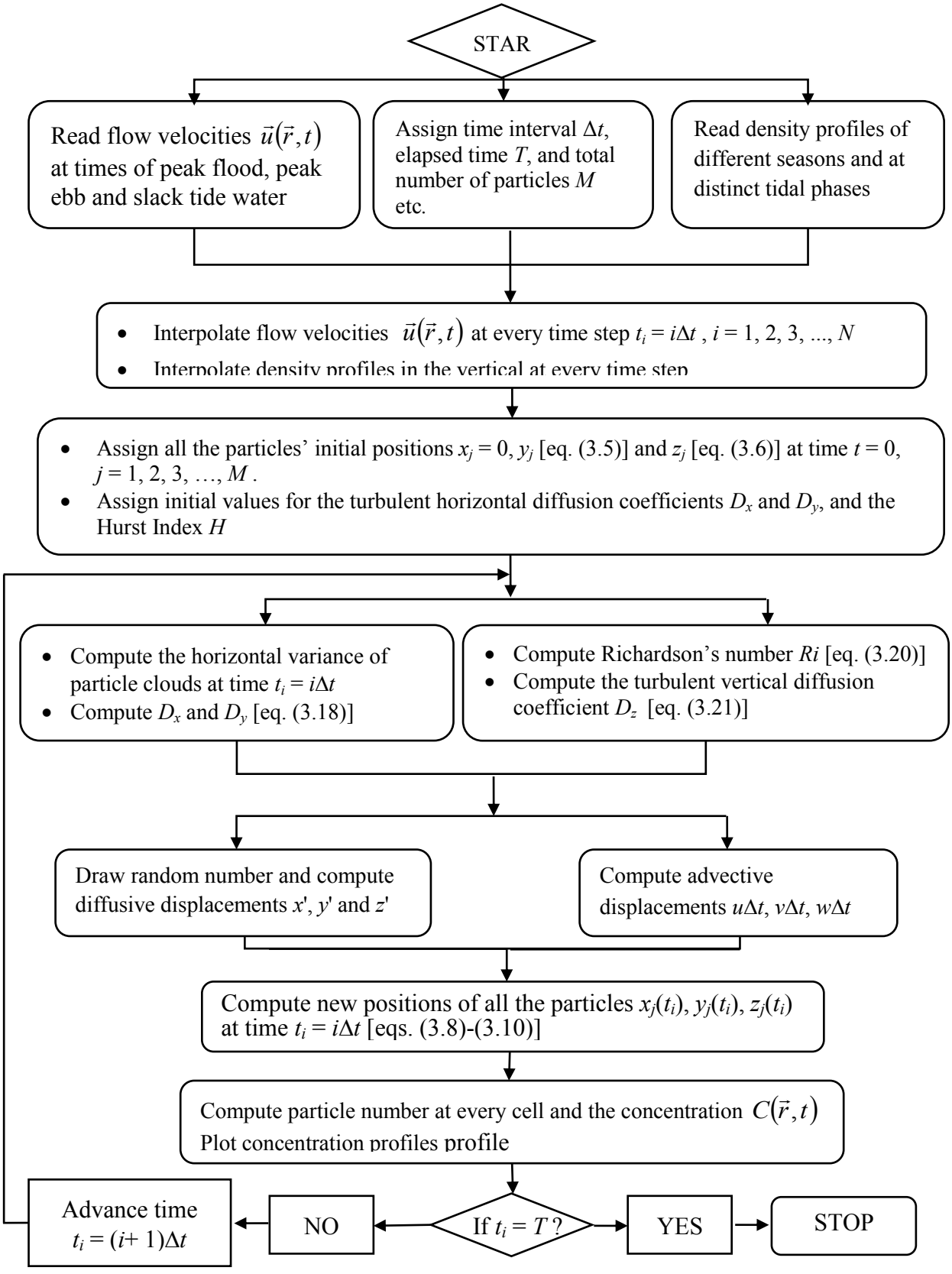

Figure 5.1 Conceptual flow chart of particle-tracking simulations.

Table 5.1 A summary of model parameters and assigned values.

Physical quantity	*Value*	*Unit*
Brunt-Väisälä frequency N	varying	s^{-1}
Concentration C	varying	ppb
Constant c_1 in Eq. (3.21)	0.001	
Constant in c_2 Eq. (3.21)	1.0	
Diffuser length L	40	m
Elapsed time T	varying	sec.
Flow velocity along-channel u	varying	m/s
Flow velocity cross-channel v	varying	m/s
Flow velocity on vertical direction w	varying	m/s
Initial value for the turbulent diffusion coefficient D_x	0.5	m^2/s
Initial value for the turbulent diffusion coefficient D_y	0.5	m^2/s
Initial variance $\sigma_\circ^2$	1	m^2
Integrated time interval Δt	4.968	Min.
Min. value for the vertical diffusion coefficient D_z	0.0001	m^2/s
Near-field trapping depth z_o	12	m
Particle settling velocity s	0	m/s
Random variate ξ	-0.5 to 0.5	
Reference density of seawater $\rho_\circ$	1000	kg/m^3
Richardson Number Ri	varying	
Standard deviation σ	1	
Time period of particle release t_d	168	Min.
Total depth of flow d	22	m
Total number of particles M	20000 or 50000	
Water level η	varying	m
Variance of particles position σ^2	varying	m^2
Variance of particles position at initial time σ_0^2	varying	m^2

Prior to a loop for computing the advective and diffusive displacements of individual particles from their initial positions, we assign initial values for the turbulent diffusion coefficients D_x and D_y in the horizontal. In those simulations where Fickian diffusion is used or the Hurst index H = 0.5, the coefficients remain the same values throughout the simulation periods. Otherwise, the horizontal coefficients are updated within the loop. Regardless of the Hurst index value, the vertical diffusion D_z is updated within the loop, depending on the Richardson number.

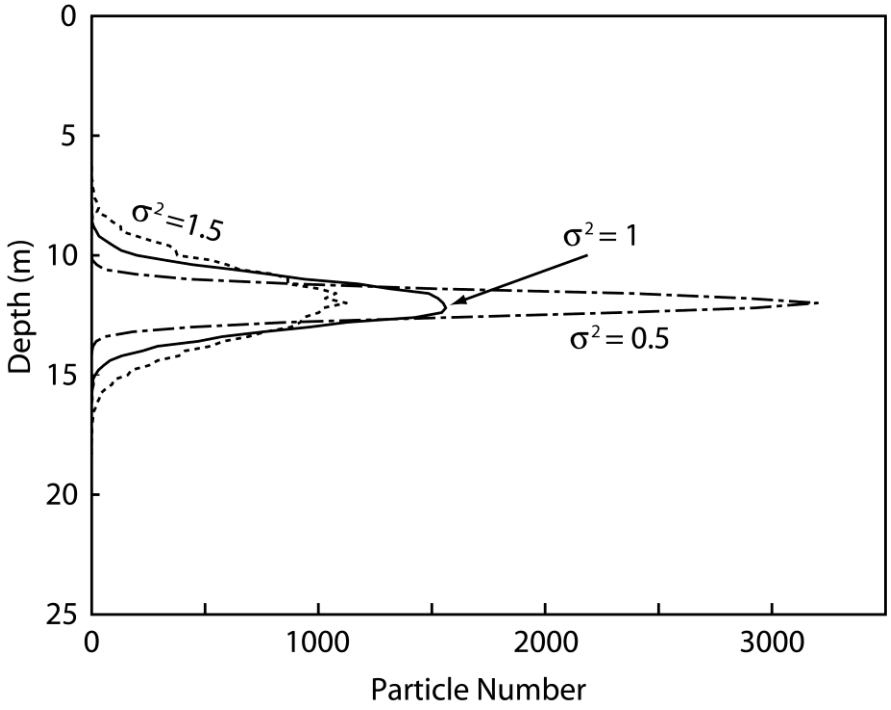

Figure 5.2 Comparison of normally distributed particles in the vertical between different values for the variance. The total number of particles is 20000.

5.2 Model Runs

A total of 20 model runs (Table 5.2), using Fickian formulisation for horizontal turbulent diffusion, are carried out. These runs will permit a comparison between numerical results and field measurements of dye concentration and will reveal to what extent Fickian formulisation can capture effluent dispersion in a tidal channel like

Burrard Inlet. For simplicity, the turbulent diffusion coefficients are assumed to be equal in the *x*- and *y*-directions. The coefficients are given a series of values in the range of 0.3 to 1.0 m^2/s. The most realistic value will be determined based on the comparison between field data and numerical results. In all the cases, the discharge of effluents is continuous.

The starting time $t = 0$ of the model runs is always at slack water immediately following either High High Water or High Low Water (Figure 5.3). The time step for particle tracking is $\Delta t = 4.968$ minutes. The simulation periods range from $8\Delta t$ to $32\Delta t$; they are chosen such that at the ending time of an individual run, the tidal phase matches that at which the selected dye-concentration profile was made. Four dye-concentration profiles (Table 5.2) are selected from the profiles observed in the inlet water during the dye-tracing surveys conducted on September 26, 1998 (Seaconsult and EVS 1998). The four observed profiles are 11d, 25u, 39u and 43d. They can directly be compared to profiles to be extracted from numerical results at the end of the model runs.

A total of 47 model runs (Table 5.3), using non-Fickian formulisation for horizontal turbulent diffusion, are performed. Similar to the Fickian diffusion runs (RF1 to RF20), these non-Fickian runs have the same turbulent diffusion coefficients in the *x*- and *y*-directions. The starting time $t = 0$ of these runs is at slack water following either High High Water or Low High Water. These runs are designed to answer the following questions:

- To what extent does non-Fickian formulisation improve particle-tracking simulations of wastewater dispersion in coastal waters?
- What is the reasonable range of Hurst index values?
- What time steps are acceptable for particle-tracking simulations?

With these questions in mind, we use a range of Hurst index (0.55 to 0.7) and various time steps for particle-tracking. Particle distribution profiles to be extracted from model results at the end of the non-Fickian runs will directly be compared to the corresponding observed dye-concentration profiles listed in Table 5.3.

Table 5.2 A list of model runs (RF1 to RF20) using Fickian diffusion. Δt = 4.968 (min).

Simulation Period (T)	Horizontal diffusion coefficients (m^2/s) ($D_x = D_y$)					Observed dye-concentration profile for comparison
	0.3	0.4	0.5	0.8	1.0	
10Δt	RF1	-	RF2	-	RF3	No.11d
24Δt	RF4	RF5	RF6	RF7	RF8	No.25u
8Δt	RF9	-	RF10	-	RF11	No.39u
12Δt	RF12	RF13	RF14	RF15	RF16	No.43d
32Δt	RF17	RF18	RF19	-	RF20	-

Table 5.3 A list of model runs (RN1 to RN47) using non-Fickian diffusion. Δt = 4.968 (min), $\Delta t_1 = \Delta t/2$ and $\Delta t_2 = \Delta t /4$.

Simulation Period (T)	Hurst index H							Observed dye-concentration profile for comparison
	0.55	0.575	0.6	0.625	0.65	0.675	0.7	
30Δt	RN1	RN2	RN3	RN4	RN5	RN6	RN7	
60Δt_1	RN8	-	RN9	-	RN10	-	RN11	
120Δt_2	RN12	-	RN13	-	RN14	-	RN15	
10Δt	RN16	-	RN17	-	RN18	-	RN19	No.11d
24Δt	RN20	-	RN21	-	RN22	-	RN23	No.25u
8Δt	RN24	-	RN25	-	RN26	-	RN27	No.39u
12Δt	RN28	-	RN29	-	RN30	-	RN31	No.43d
20Δt_1	RN32	-	RN33	-	RN34	-	RN35	No.11d
48Δt_1	RN36	-	RN37	-	RN38	-	RN39	No.25u
16Δt_1	RN40	-	RN41	-	RN42	-	RN43	No.39u
24Δt_1	RN44	-	RN45	-	RN46	-	RN47	No.43d

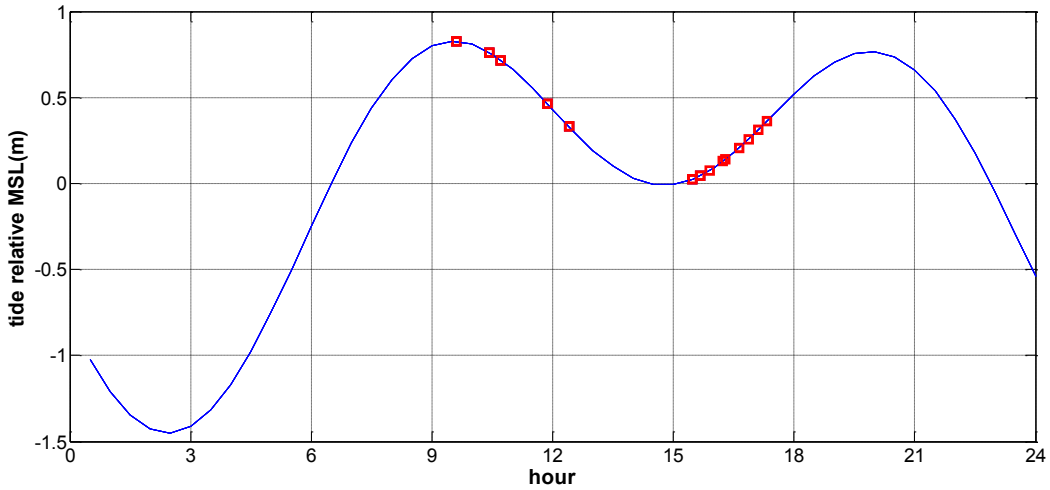

Date: September 26, 1998

Figure 5.3 Time series of water level (η) at Pt. Atkinson in Burrard Inlet. Slack water occurred about 10 minutes following High High Water (shortly after 09:00 PDT) and High Low Water (around 15:00 PDT). The squares indicate the times of dye concentration sampling in the WWTP during the dye-tracing surveys (Figure 4.2).

5.3 Time-dependent Ambient Flow

The water level in Burrard Inlet, as obtained from harmonic predictions for 26 September 1998, shows fluctuations in time (Figure 5.3). This is due to tidal waves that propagate to the inlet. The tides have four major constituents, namely M_2, S_2, K_1 and O_1, and are classified as predominantly semidiurnal (Thomson, 1981). The time series plotted in Figure 5.3 shows two occurrences of High High Water, one occurrence of Low Low Water and once occurrence of High Low Water. In the inlet the ambient flow is driven mainly by the tides and is modified by forcing related to density variation and by the presence of irregular shorelines. Accordingly, the ambient flow varies continuously in time.

For particle-tracking modelling, ambient flow velocities over the entire model domain at every time step are needed [Eqs. (3.1)–(3.3)], but such details of the ambient velocity field are not directly available from field observations. In this study the detailed velocity field is constructed as described below. Three velocity profiles, observed in the vicinity of the diffuser at three distinct tidal phases, are selected from the ADCP measurements made during the field survey (Figure 4.2), which was discussed in Section 4.3.2. The distinct tidal phases are peak flood, slack water and peak ebb; the corresponding velocity profiles are plotted in Figures 5.4a-c. These profiles show the streamwise current speeds in the dominate direction of flood/ebb flow. The current speeds vary with depth due to the influences of the seabed friction as well as the density-induced forcing on the otherwise vertically uniform tidal flow.

The three profiles were measured at a location near the diffuser in First Narrows (Figure 4.2). They are assumed to be representative for the entire narrow channel. This assumption is supported by the flow patterns shown in Figures 4.3a-d. In order to give approximate flow velocities at any required time step or any other tidal phase other than peak flood, slack water and peak ebb, we use linear interpolation on the profiles. Linear interpolation in time does introduce small errors since tidal variations are non-linear (e.g. sinusoidal), as illustrated in Figure 5.3.

It is worth noting that the slack–water profile (Figure 5.4b) shows weak velocities (about 10 cm/s) near the surface. The peak-flood and peak-ebb profiles show a maximum velocity of 30 and 54 cm/s, respectively. In both cases the velocities change significantly with depth; this has important implications for calculations of the vertical turbulent diffusion coefficient D_z [Eq. (3.21)].

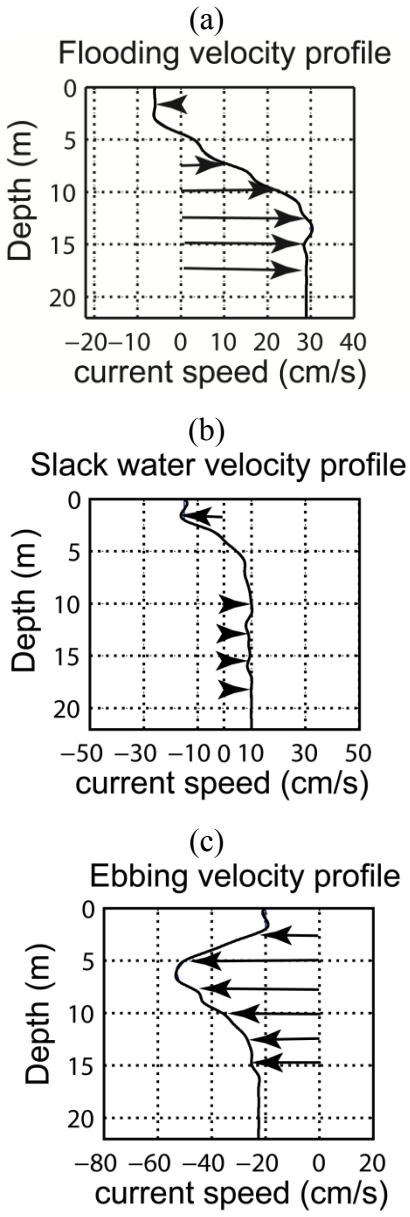

Figure 5.4 Observed profiles of ambient flow velocity at three distinct tidal phases: peak flood, slack water and peak ebb (modified from Seaconsult & EVS, 1999). The positive and negative values for speed correspond to flood tide and ebb tide, respectively (see Figure 4.1).

5.4 Density Profile

In this study, particle-tracking modelling allows for variations in the density of ambient water with both depth and time (or equivalently tidal phase). Two density profiles are selected from the CTD measurements made during the field survey described in Section 4.3.2. The profiles are plotted in Figures 5.5a,b as σ_t, which is defined as the density of ambient water in kg/m^3 minus 1000. Both profiles show significant variations in ambient density with depth, ranging from $\sigma_t = 0$ (fresh water) near the surface to about $\sigma_t = 21$ (the density of seawater under normal conditions) at 10 m below the water surface or deeper. The vertical structure affects the Brunt-Väisälä frequency N and hence the Richardson number Ri [Eq. (3.20)], and further affects the vertical turbulent diffusion coefficient D_z [Eq. (3.21)].

The two density profiles (Figures 5.5a,b), measured at a location near the diffuser in First Narrows (Figure 4.2), are assumed to be representative for the entire narrow channel. This assumption is justified by the fact that within First Narrows turbulent mixing in the horizontal is intensive, making the density field spatially uniform in the horizontal (Li and Hodgins, 2010).

In terms of temporal variations of the density field, the two density profiles correspond to peak flood and peak ebb, respectively. Approximate density profiles for all other tidal phases are obtained by using linear interpolation on the two profiles over time. These approximations allow us to compute the diffusion coefficient D_z [Eq. (3.21)] at all time steps of a particle-tracking simulation. Note that the flood profile (Figure 5.5a) shows a sharp change just below 5 m from the water surface, whereas the ebb profile (Figure 5.5b) varies nearly linearly with depth over the top 12 m.

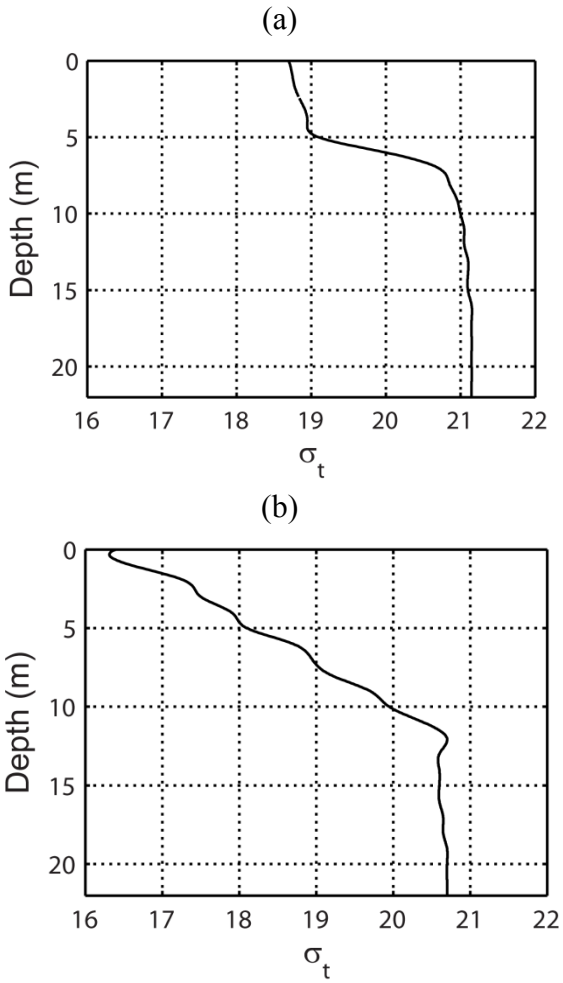

Figure 5.5 Vertical structures of the ambient density field: (a) at peak flood; (b) at peak ebb (modified from Seaconsult & EVS, 1999).

CHAPTER 6 RESULTS AND DISCUSSION

6.1 Introduction

This chapter is devoted to the presentation of numerical results for the model runs whose conditions are given in Chapter 5. A comparison between the numerical results and field data will be shown to demonstrate the predictability of the particle-tracking model described in Chapter 3. We will begin with presenting the general features of model predictions in Section 6.2. To facilitate comparisons between predicted particle distributions and observed concentration profiles, it is necessary to make a proper conversion. The procedures for the conversion will be discussed in Section 6.3.

The results for model runs with Fickian diffusion in the horizontal (Table 5.2) will be compared with field data in Section 6.4. Through these comparisons, one appreciates why it is important to incorporate density stratification in the formulisation of the vertical turbulent diffusion. In this regard, the focus is on the vertical structures of wastewater effluents at a series of horizontal distances from the source.

The model results for the runs using non-Fickian diffusion in the horizontal (Table 5.3) will be presented in Section 6.5, and compared with field data. Through these comparisons we will discuss in Section 6.6 how the Hurst index affects particle dispersion in a tidal channel. The issue about to what extent the choice of an integration time interval matters in particle-tracking modelling under continuous release will be addressed in Section 6.7. This chapter will end with discussion about the decay of maximum concentration with distance from the source, which has relevance to the compliance to water quality regulation by a given outfall discharge.

6.2 Simulated Distribution of Particles

The output from a model run contains the (x, y, z) coordinates of individual particles at every time step over a specified simulation period. An example of simulated distributions of particles is shown in Figure 6.1. This shows the positions in three-dimensional space of a total of 5000 particles that are continuously released into the ambient water over a period of about 168 minutes. These particles are initially located at x = 1000 m (the source location), and arrive at different locations due to advection and turbulent diffusion. The ambient flow is flooding in the positive direction of the x axis. Depending on the time elapsed following the release from its initial position, a particle may remain in the model channel or reach the channel boundaries (Figure 6.1). Particles that have reached the channel side boundaries or are 1000 m or more in longitudinal distance away from the source are considered to have left the model channel and are no longer tracked in order to reduce the computational cost.

In particle-tracking modelling, it would be preferred to use as small time interval as possible. For most simulations we use a time interval Δt equal to 4.968 min. On one hand, this time interval gives a reasonable computational efficiency. On the other hand, the M2 tidal period of 12.42 hours is conveniently divided into 150 time steps.

An important feature shown in Figure 6.1 is that the plumes are submerged below the water surface. This qualitatively confirms the predictability of the model for wastewater effluent dispersion in density-stratified coastal waters. Submerged dispersion in density-stratified ambient waters has been observed in laboratory experiments (see Figure 2.1b) and in the field (e.g. Li and Hodgins 2010). Wastewater effluents neither penetrate to the water surface nor come to contact with the bottom. This is a preferred

scenario from the perspective of protecting the recreational use of local surface water and the benthic community. It is important to note that the prediction of no bottom-contact is under the assumption of zero settling velocity. Nevertheless, an extension of this study to include settling velocity is straightforward.

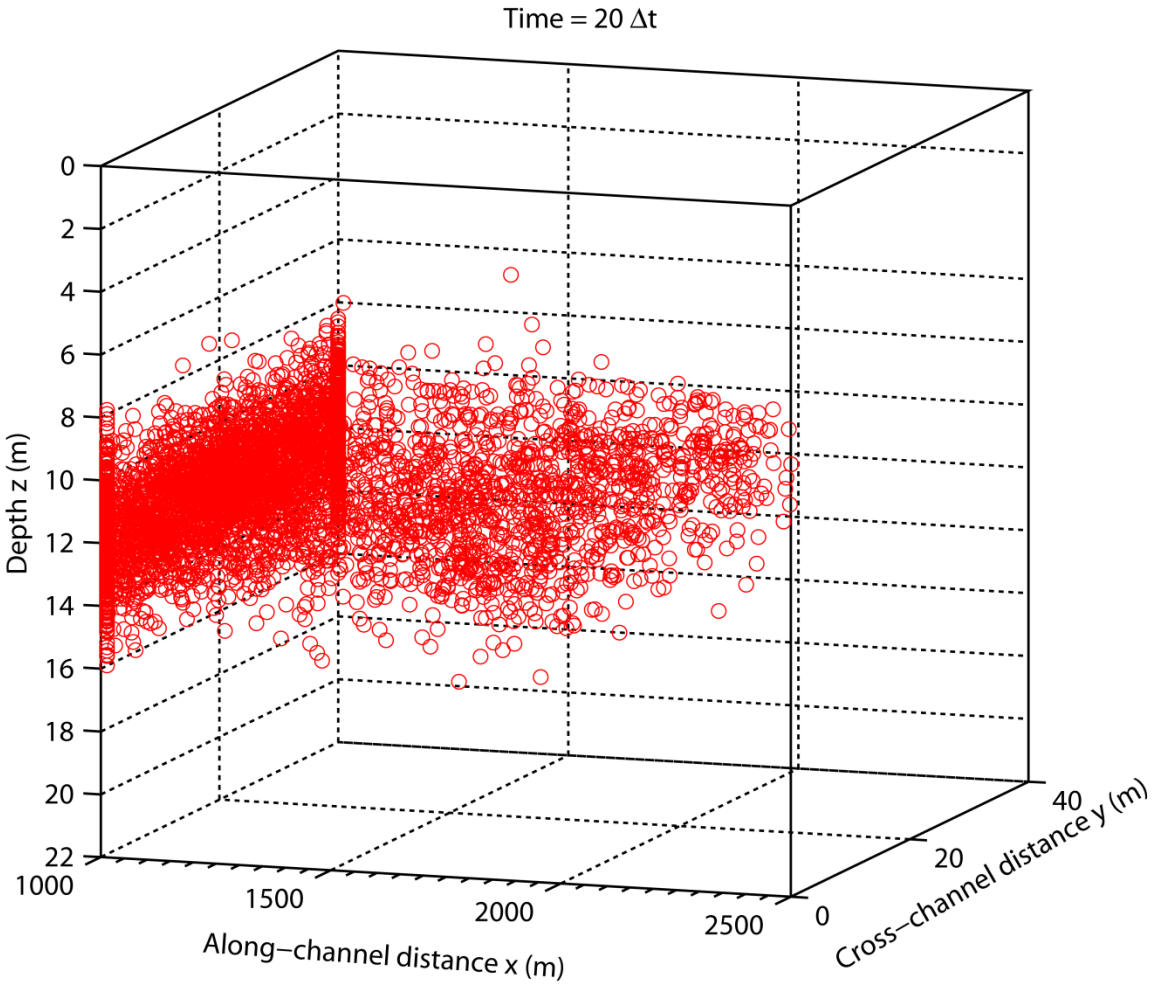

Figure 6.1 Simulated distribution of 5000 particles in three-dimensional space at time $T = 20\Delta t$. The simulation conditions are: Δt is 4.968 min., t_d is 168 min., the initial value for D_x and D_y is 0.5 m^2/s and the initial value for D_z = 0.001 m^2/s. The source is located at x = 1000 m. The ambient flow is flooding. The density is stratified.

6.3 Conversion between Particle Distribution and Concentration Field

Particle-tracking modelling does not provide concentration. In order to compare predicted distributions of particles and observed effluent concentrations, it is a matter of necessity to sample particles within a volume of ambient water where the effluent concentrations are observed. In this regard there are two things that bear emphasising. Firstly, the sampling volume should be reasonably large so that it will contain enough particles for determining their spatial distributions without a discontinuity problem. Second, the correspondence between particle distribution and effluent concentration must be established.

In this study the sampling volume is chosen to have the dimensions of Δx = 1m, Δz = 0.5 m and Δy equal to the diffuser length. The dimension in the cross-channel y-direction is not critical, because in this direction the distribution of particles is more or less uniform. If an observed concentration profile to be compared is from a location where the along-channel coordinate is $x = x_p$, a total of 44 rectangular sampling volumes are made stacking in the z-direction and centred at x_p. The middle z-coordinates of the sampling volumes are 0.5, 1, 1.5, ..., 21.5 m below the water surface, respectively. The number of particles within each sampling volume can be counted and plotted on the horizontal axis against the middle z-coordinate on the vertical axis, to show the vertical distribution of particles.

The correspondence between particle distribution and effluent concentration is established as follows. The peak concentrations of the four observed profiles (11d, 25u, 39u and 43d), listed in Table (5.2) and plotted in Figures 6.2a-d, are identified, being 26.6, 29, 24 and 15.5 ppb, respectively. The four runs RF1, RF4, RF9 and RF12 have an

end time matching, respectively, the four observed profiles in terms of tidal phase. For each of the four runs particle positions at the simulation ending time are available. The number of particles within vertically stacking sampling volumes that match the individual observed profile in terms of location is counted, and the particle number maximum is identified. In Figure 6.3, we plot the observed peak concentrations on the horizontal axis and the predicted particle number maxima on the vertical axis. The particle number maxima are 59, 47, 31 and 42 for runs RF1, RF4, RF9 and RF12, respectively. This set of model runs use horizontal diffusion coefficients $D_x = D_y = 0.3$ m^2/s. In Figure 6.3, we also plot the predicted particle number maxima for the runs with $D_x = D_y = 0.5$ m^2/s (RF 2, RF6, RF10 and RF14) and for the runs with $D_x = D_y = 1.0$ m^2/s (RF3, RF8, RF11 and RF16).

An overall linear-fitting line is plotted through the data points, which has a slope of 1.8. The slope of the line should be interpreted as the multiplying factor for the conversion from effluent concentration to particle number. Nevertheless, it is important to note that since all model runs involve a random process, slightly different values for the slope are expected from different sets of model runs. After some test runs, we determine the scale factor as 2. This value will subsequently be used as the conversion factor. Although the conversion factor is based on peak concentrations, this is justified by the fact that it is the high-concentration core of wastewater plumes that causes a water-quality problem.

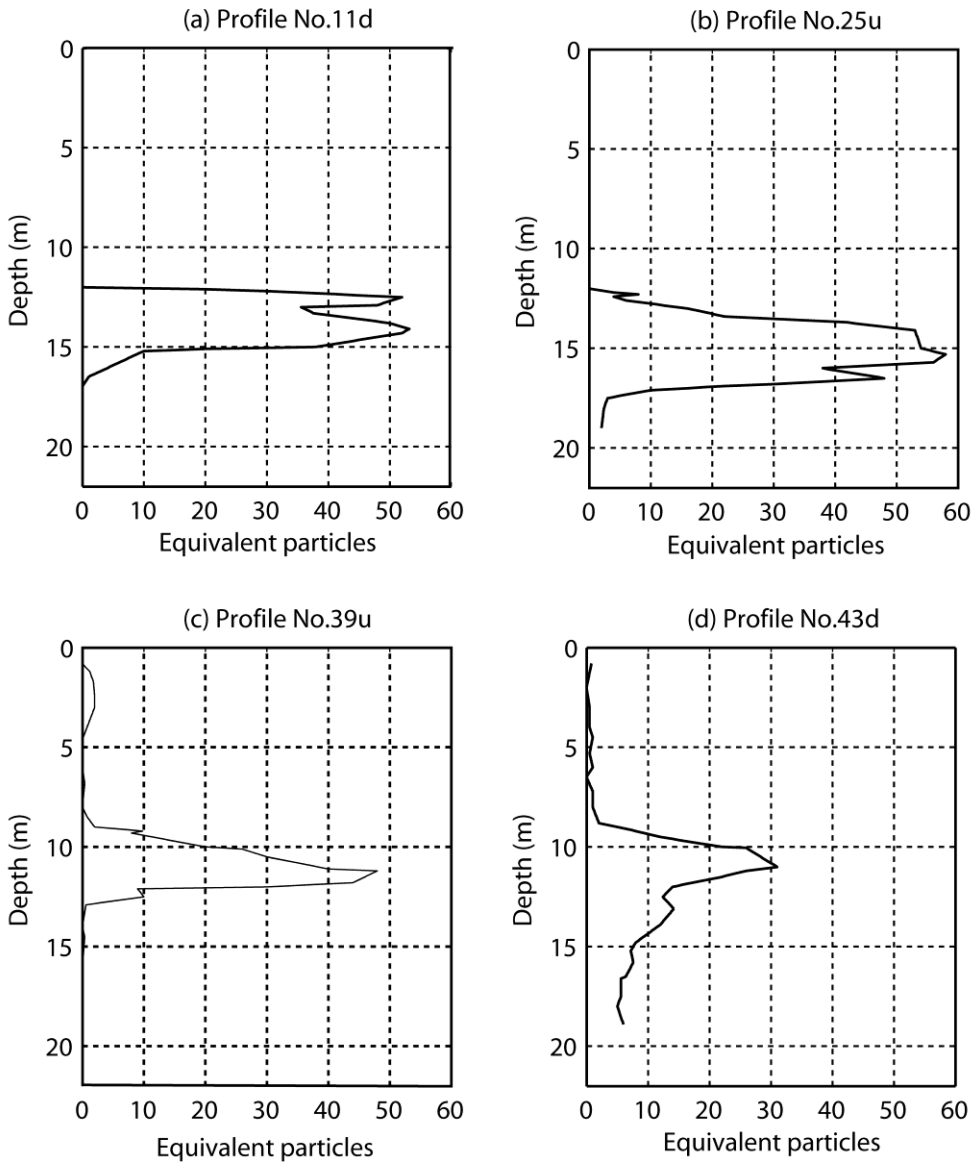

Figure 6.2 Profiles of dye concentration observed on 26 Sept. 1998. The locations, in easting and northing relative the midpoint of the diffuser, are: (a) (-24 m E, -28 m N), (b) (-166 m E, 64 m N), (c) (129 m E, -36 m N), and (d) (367 m E, -214 m N), respectively.

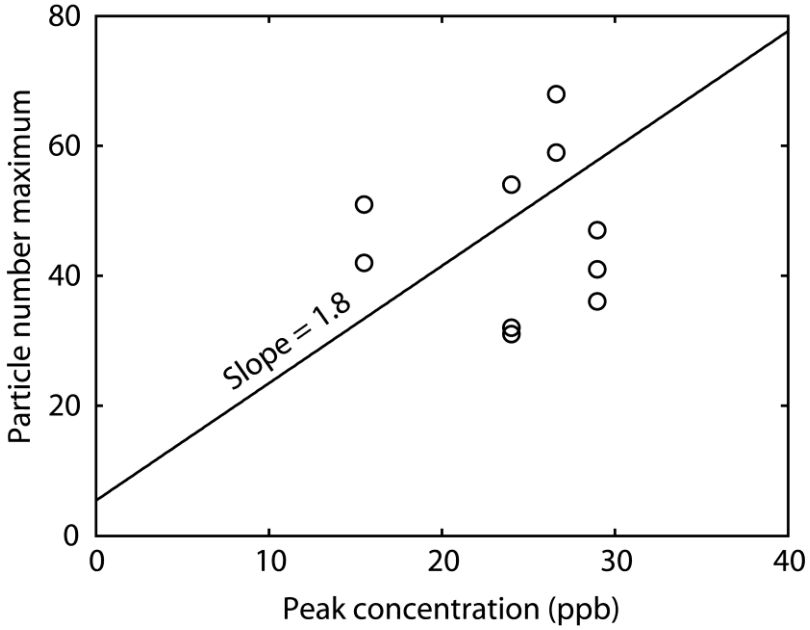

Figure 6.3 Observed peak concentration vs. predicted particle number maximum.

6.4 Simulation Results with Fickian Diffusion

The vertical distributions of particles are sampled from the numerical results of the Fickian runs listed in Table 5.2, at times and in locations corresponding to the observed concentration profiles shown in Figures 6.2a-d. The vertical distributions are shown as the dashed curves in Figures 6.4a-c to 6.7a-c. The observed concentration profiles are converted to particle number distributions and are plotted in the figures for comparison. In Figures 6.4a-c, the observed profile (11d) shows a plume core of high concentrations about 3 m thick (from depth z = 12.05 to 15.2 m); this core thickness is well matched by the model prediction. The thicknesses of the plume core seen in the other profiles (25u, 39u and 43d) are also correctly predicted by the model (Figures 6.5a-c to 6.7a-c); the three observed profiles show a plume core of approximately 5, 3 and 6 m thick, respectively.

The vertical locations of the predicted and observed plume cores are either overlapped or partially overlapped (Figures 6.4a-c to 6.7a-c). In the case of a partial overlap, the differences are within 1 to 3 m in vertical distance; this is acceptable in comparison to the total depth of flow of 22 m. Specifically, in Figure 6.4a-c and 6.5a-c, the observed plume cores are plotted below the predicted ones. This can be explained by the fact that the model channel is an idealised channel with a flat bottom, whereas the real bottom topography at the two locations has a downward slope in the direction of ebbing flow (Figure 4.2 and Figures 4.3c,d). The ebbing flow is expected to have a downward velocity component [or $w < 0$ in Eq. (3.10)], which would cause the plume core to deepen. However, due to data limitation, our simulations assume the vertical velocity component to be zero. In fact, the vertical component of the ambient velocity field is difficult to measure in the field and to predict in hydrodynamics modelling, although more realistic bottom topography with longitudinal variations can easily be accommodated in our particle-tracking model.

Most importantly, these comparisons evidence that the particle tracking model is capable to realistically reproduce sharp variations in concentration. The predictions capture such detailed features as the double peaks exhibited in profile 11d and the subtle variations near the upper and lower edges of the bell-shaped curve seen in profile 39u. Profile 43d shows relatively high concentrations below the peak value, which is not seen in the prediction, possibly because settling velocity in the vertical is not considered in the present study.

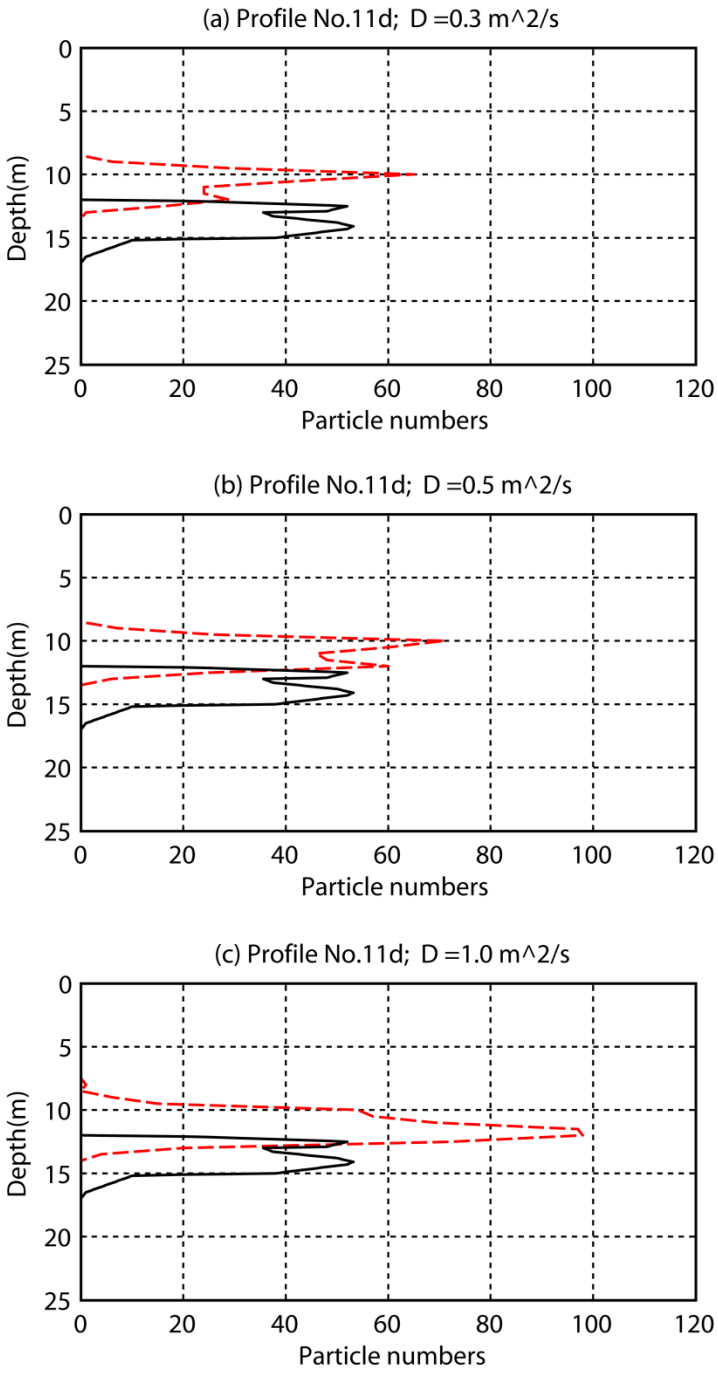

Figure 6.4 Comparison of the vertical structures between field observation (solid curve) and numerical prediction (dashed curve) for runs RF1 (panel a), RF2 (panel b) and RF3 (panel c).

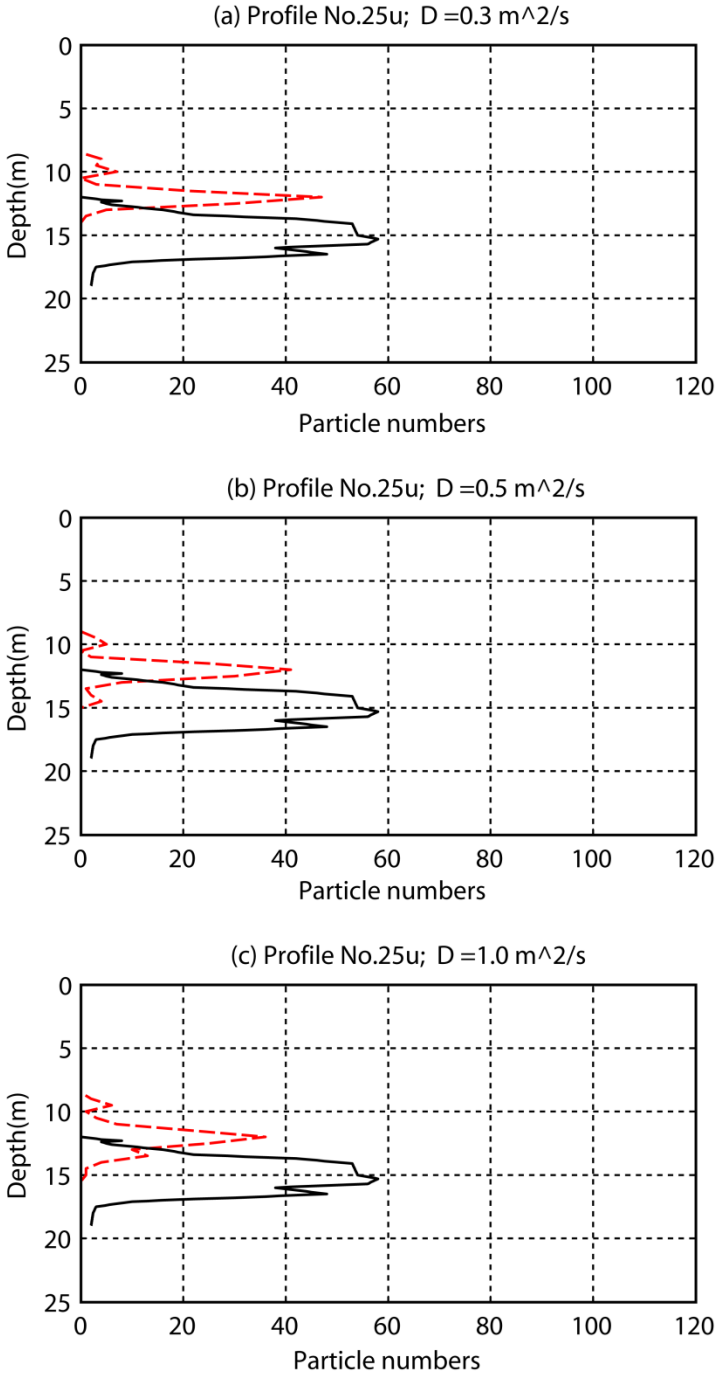

Figure 6.5 Comparison of the vertical structures between field observation (solid curve) and numerical prediction (dashed curve) for runs RF4 (panel a), RF6 (panel b) and RF8 (panel c).

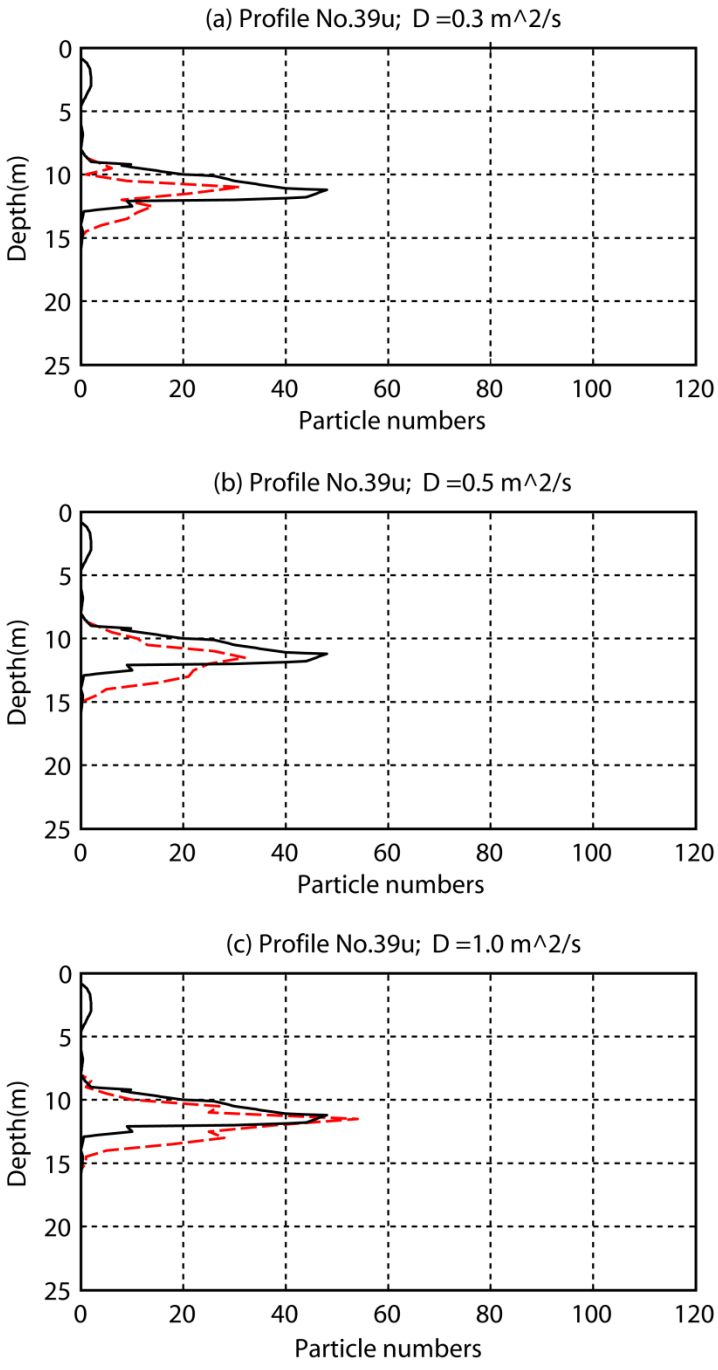

Figure 6.6 Comparison of the vertical structures between field observation (solid curve) and numerical prediction (dashed curve) for runs RF9 (panel a), RF10 (panel b) and RF11 (panel c).

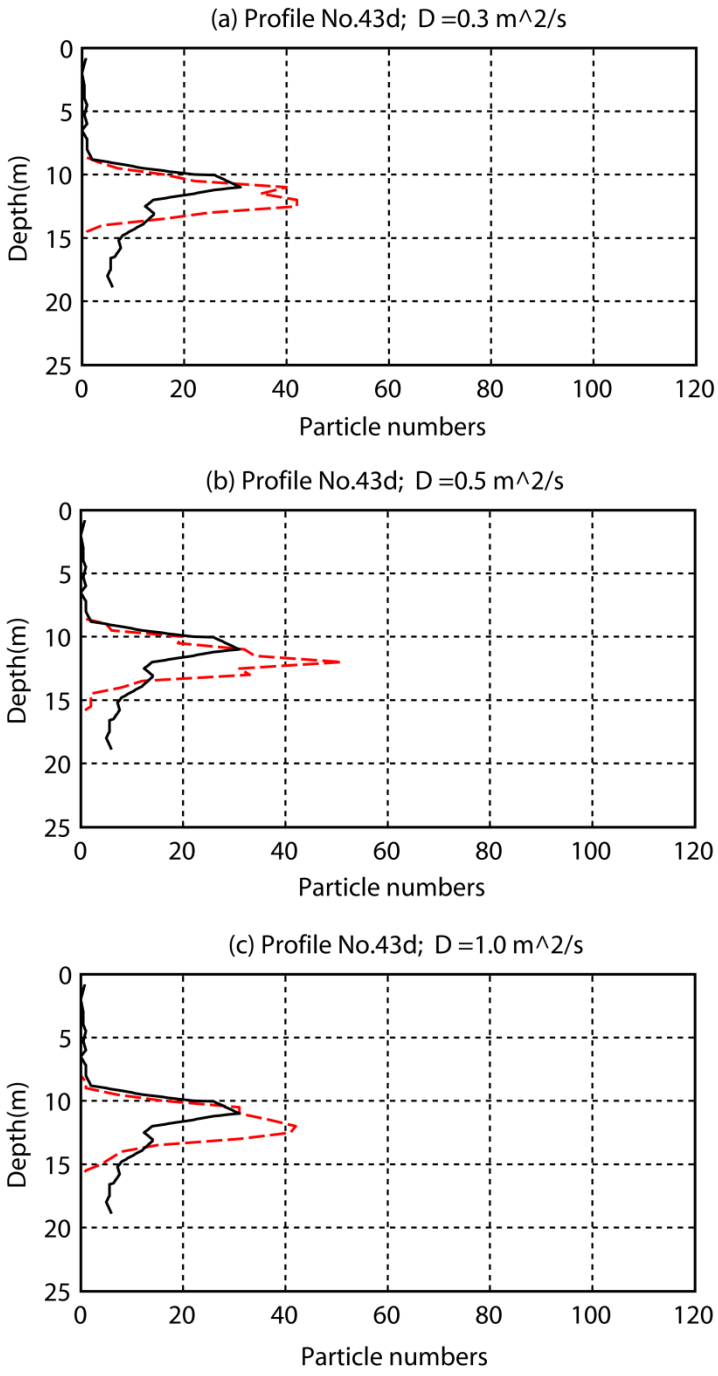

Figure 6.7 Comparison of the vertical structures between field observation (solid curve) and numerical prediction (dashed curve) for runs RF12 (panel a), RF14 (panel b) and RF16 (panel c).

Overall, the predicted peak values (or particle number maxima) are in reasonable agreement with the observed ones, as shown in Figures 6.4a-c to 6.7a-c. It appears that using a value of 0.3 or 0.5 m^2/s for the horizontal diffusion coefficients makes predictions of the peak value (or particle number maximum) closer to the field data than using a value of 1.0 m^2/s for the coefficients. Recall that the model runs RF1, RF2 and RF3 differ in that the horizontal diffusion coefficients increase from $D_x = D_y = D = 0.3$ to 0.5 to 1.0 m^2/s. The predicted peak values appear to increase with an increasing value for the coefficients, and the run RF3 predicts the highest peak value (Figures 6.4a-c). The same trend is seen in Figures 6.6a-c, whereas the opposite trend is seen in Figures 6.5a-c. In Figures 6.7a-c, the predicted peak values appear insensitive to the values for the coefficients. It is unclear why this has occurred. Generally speaking, in Eulerian simulations, one expects that an increasing value for the diffusion coefficients will lead to a decreasing peak concentration. For an optimal prediction of particle number maxima, a value of 0.5 m^2/s is recommended for the horizontal diffusion coefficients.

Our success in predicting the plume structures as illustrated above is attributed to the key idea of formulating the vertical diffusion coefficient as a function of velocity shear and density stratification. Particle random walks in the vertical or equivalently turbulent mixing activities in the vertical of wastewater effluents with the ambient water are inhibited by density stratification. We suggest that this must be taken into account in particle-tracking modelling.

To confirm this suggestion, we conducted three model runs where the diffusion coefficients are constant. In all the three runs, the horizontal diffusion coefficients are the same ($D_x = D_y = D = 1.0$ m^2/s), whereas the vertical diffusion coefficient is $D_z = 0.001$,

0.01 and 0.1 m^2/s, respectively. This is Fickian diffusion formulisation, because there are no spatial or temporal variations in the diffusion coefficients. Other conditions are the same as in model run RF11 (see Table 5.2).

The numerical results for the three runs are compared to the field data in Figure 6.8. Even if the vertical diffusion coefficient is given a value as low as $D_z = 0.001 m^2/s$, the model predicts a broaden plume core, compared to the observed concentration profile. If D_z is increased to 0.01 m^2/s, the predicted plume core broadens to such an extent that the prediction no longer reflects the observed shape. A further increase of the coefficient to 0.1 m^2/s completely destroys the vertical structure. We conclude that using a constant vertical viscosity will not be able to realistically simulate particle dispersion in density-stratified coastal waters.

Values of the vertical diffusion coefficient D_z in the range of 10^{-4} to10^{-3} m^2/s are reported to be a robust estimate of vertical diffusivity within the ocean waters. According to Cisewski *et al.* (2005), values in the top mixed layer are more variable in time and reach 10^{-1} m^2/s during periods of strong winds. However, the use of a constant vertical diffusion coefficient is not suitable for particle-tracking modelling. Even if the coefficient is given a small value, the vertical structure of simulated plumes will disappear after a few tidal cycles. For realistic particle dispersion simulations, the vertical diffusion coefficient should be given a small initial value, for instance $D_z = 0.001 m^2/s$ (in this study), and should be allowed to vary in time and space. The formulisation given in Eqs. (3.20)–(3.21) is relevant to ambient conditions characterized by velocity shear and density stratification.

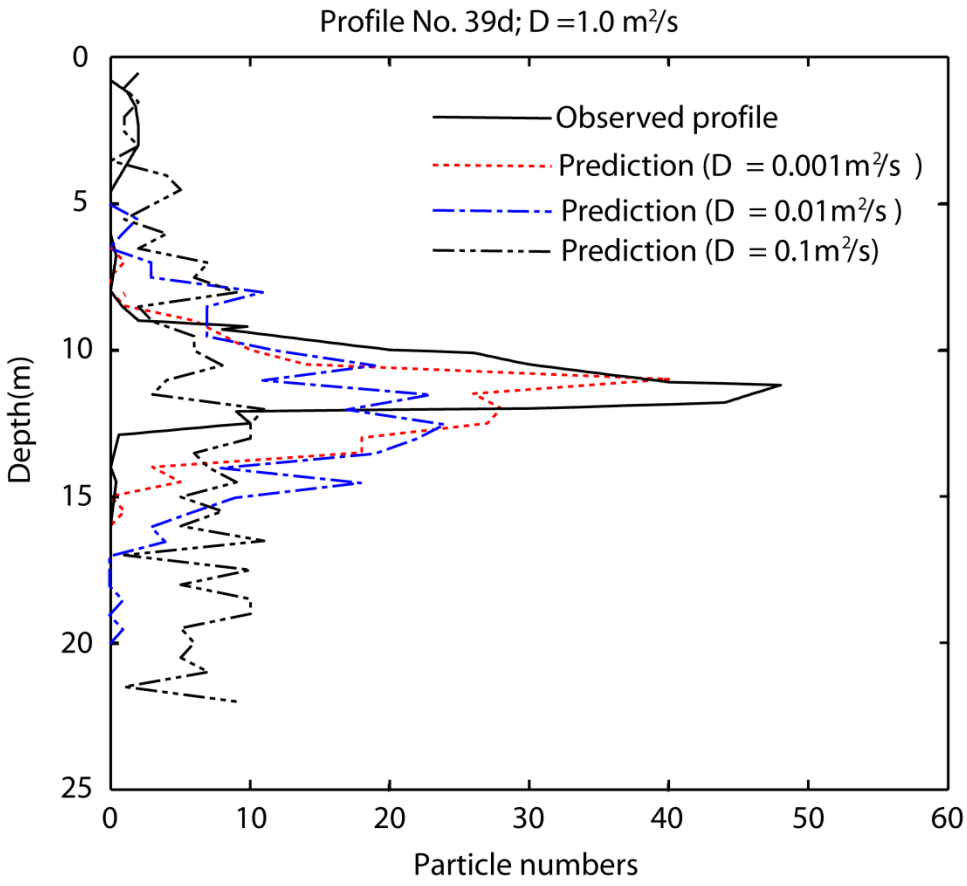

Figure 6.8 Comparison of the vertical structures between field observation (solid curve) and numerical prediction (dashed curve) for runs where all the diffusion coefficients are constant.

6.5 Model Results with Non-Fickian Diffusion

Non-Fickian model runs involve the use of the Hurst index which characterises horizontal diffusion. In the 47 non-Fickian model runs listed in Table 5.3, the Hurst index varies from 0.55 to 0.70. The lower limit may be referred to as a weak dependence of horizontal diffusion on the changing size of particle clouds or equivalently on the elapsed time of the dispersive particle clouds. Given the constriction by the shorelines on particle dispersion in the model channel (Figures 4.2 and 4.3), the upper limit may be referred to

as a strong dependence, although a value of 0.75 has been reported as being typical for coastal waters (see e.g. Addison 1997).

We closely examine the predicted vertical structures of particle distribution for different values for the Hurst index (in the range of 0.55 to 0.70). Although the vertical structures of particle distribution are more or less dictated by the formulisation of the vertical diffusion coefficient, which is dependent of the Richardson number in the study, a change of the Hurst index does have some effects on the vertical structure. It is determined that a value of 0.6 for the Hurst index produces the best match between predictions and field data. The numerical results and field data are compared in Figures 6.9 to 6.12. The results for the model runs with Fickian diffusion are also plotted in the figures for comparison. The differences in predicted vertical structure between the non-Fickian runs and the corresponding Fickian runs appear to be minor. This is perhaps because the time periods of the mode runs are short, ranging from about 40 min. (RN 21) to about 120 min. (RN25).

The effects of non-Fickian diffusion become evident only after a relatively long period of time. Possibly this is the reason for the improvement seen in Figure 6.11 made by implementing non-Fickian diffusion in the run RN25. Note that this non-Fickian run has the longest time period of the runs for which the numerical results are illustrated in Figures 6.9 to 6.12. Through comparison with the field data, we found that the Hurst index can be taken as 0.6 for the practical purposes of simulating wastewater effluent dispersion in a tidal channel with moderate ambient flow. For instance, flow velocities are on the order of 1 m/s.

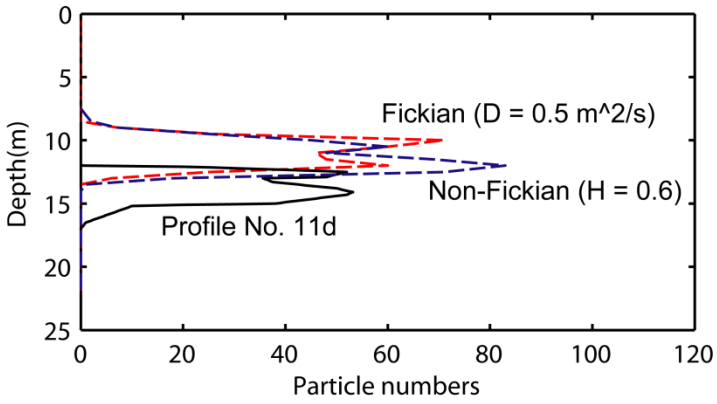

Figure 6.9 Comparison of the vertical structures between field observation 11d (solid curve) and numerical predictions for the non-Fickian diffusion run RF17 (dashed, blue curve) and for the Fickian diffusion run RF2 (dashed, red curve). The model runs are listed in Tables 5.2 and 5.3.

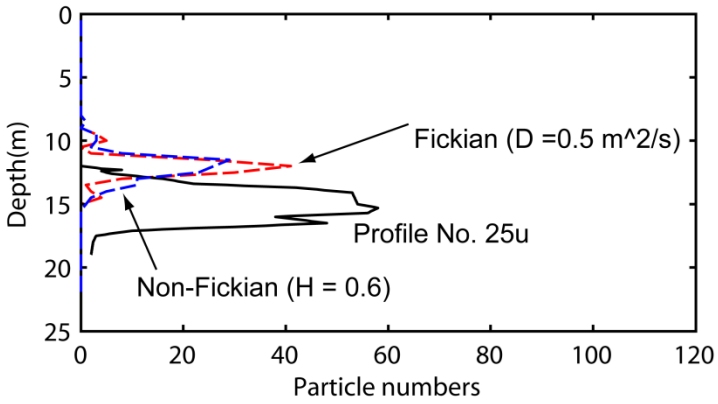

Figure 6.10 Comparison of the vertical structures between field observation 25u (solid curve) and numerical predictions for the non-Fickian diffusion run RF21 (dashed, blue curve) and for the Fickian diffusion run RF6 (dashed, red curve). The model runs are listed in Tables 5.2 and 5.3.

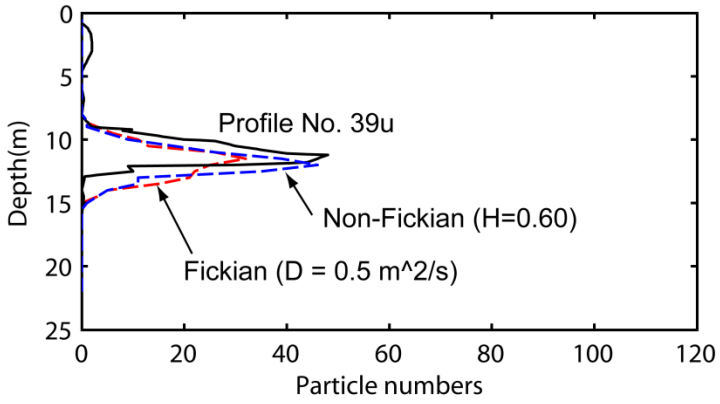

Figure 6.11 Comparison of the vertical structures between field observation 39u (solid curve) and numerical predictions for the non-Fickian diffusion run RF25 (dashed, blue curve) and for the Fickian diffusion run RF10 (dashed, red curve). The model runs are listed in Tables 5.2 and 5.3.

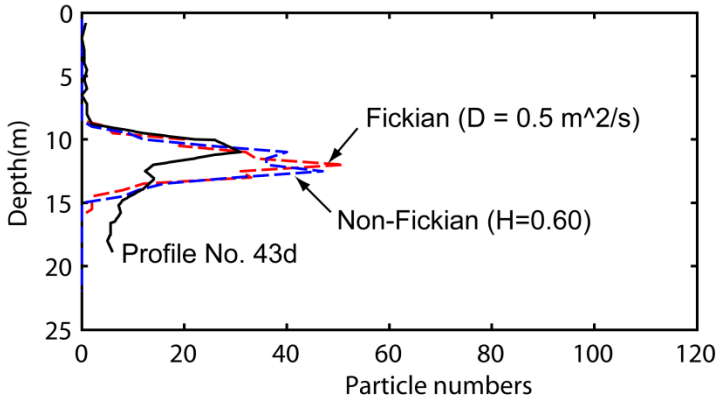

Figure 6.12 Comparison of the vertical structures between field observation 43d (solid curve) and numerical predictions for the non-Fickian diffusion run RF29 (dashed, blue curve) and for the Fickian diffusion run RF14 (dashed, red curve). The model runs are listed in Tables 5.2 and 5.3.

6.6 Effects of the Hurst Index

As a non-Fickian diffusion phenomenon, wastewater effluent plumes spread in the horizontal at a rate that increases with time. This phenomenon is simulated by the particle-tracking model using the Hurst index with values of greater than 0.5. As the Hurst index increases, there is a corresponding increase in the time rate of spreading of particle clouds or an increase in the variance of particle clouds.

This may be interpreted as individual particles being further apart from each other or as wastewater effluents being more diluted by the ambient water or as wastewater effluent concentrations becoming lower in time. The increase in the variance of the particle clouds over one tidal cycle (M2 period equal to 12.42 hours) is illustrated in Figure 6.13. The time series show that the time rate of increase is large at the initial stage of dispersion and slows down at later times, which is physically correct.

At the same time, the differences between the time series (Figure 6.13) point to the importance of obtaining a relevant value for the Hurst index for wastewater effluent disperse in coastal waters. The use of lower values for the index predicts patchy particle clouds, particularly near the source (Figure 6.14a, with $H = 0.55$). As the index increases, the patchy particle clouds trend to merge (Figure 6.14b, with $H = 0.60$). A further increase of the index results in fully mingled particle clouds (Figure 6.14c, with $H = 0.675$).

These illustrations reveal that the degree of dispersion is very sensitive to the Hurst index. The value for the Hurst index should be calibrated using field and laboratory data.

In the present study, the use of H = 0.60 appears to be suitable; numerical results and field data are in reasonable agreement.

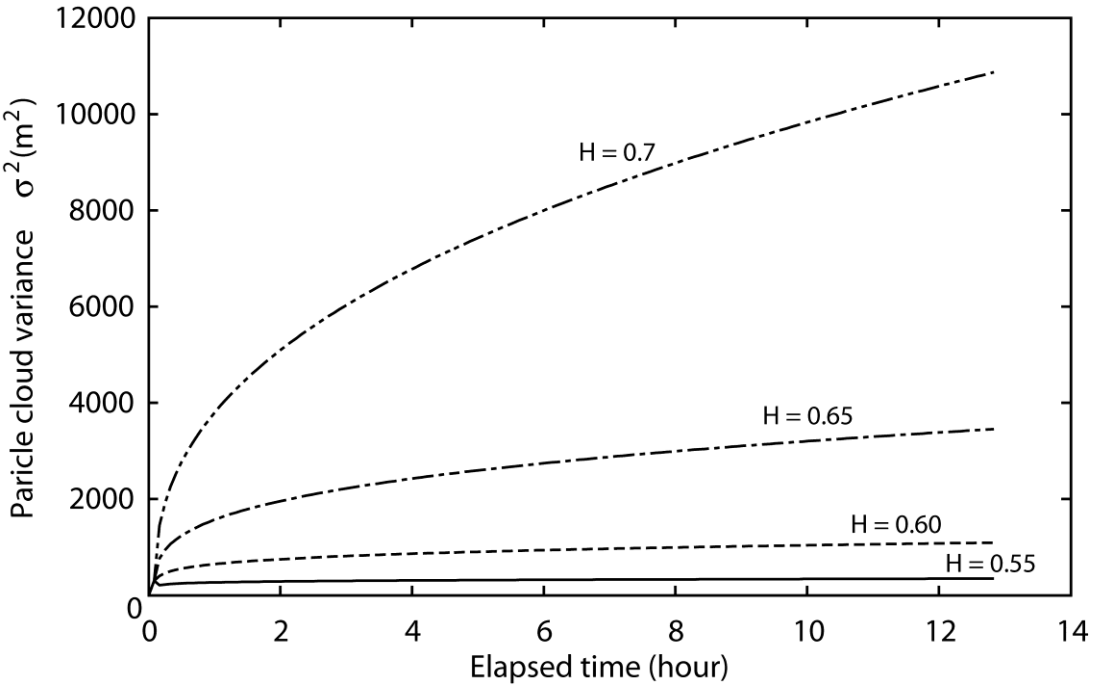

Figure 6.13 Time series of the variance of dispersive particle clouds for different values of the Hurst index.

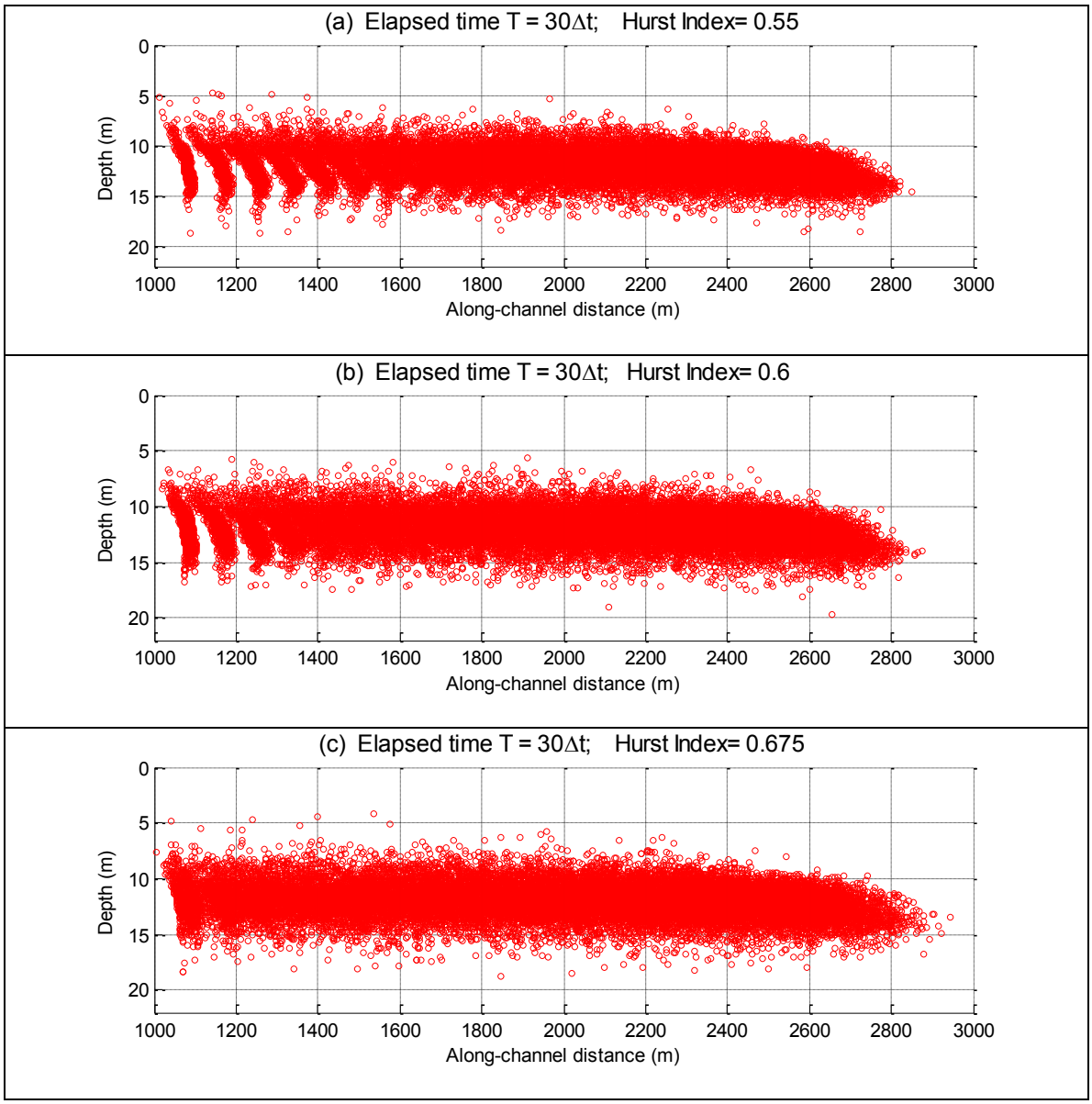

Figure 6.14 Three-dimensional distributions (viewed from the *y*-axis) of particles for non-Fickian runs with the Hurst index equal to 0.55, 0.60 and 0.675. The simulation conditions are: Δt is 4.968 min., t_d is 168 min., the initial value for D_x and D_y is 0.5 m^2/s and the initial value for D_z = 0.001 m^2/s. The source is located at x = 1000 m. The ambient flow is flooding. The density is stratified.

6.7 Integration Time Interval

In particle-tracking modelling, the integration time interval is not a parameter. Although it is desirous of using small integration time interval in order to best simulate a continuous release, there is a limit due to computational cost. On the other hand, the use of integration time intervals that are too large may produce unphysical results. One of the unphysical results is the prediction of overly patchy plumes, similar to what is shown in Figure 6.14a. Almost all the simulations in this study use a time interval of $\Delta t = 4.968$ minutes. However, we have rerun some of the simulations with the integration time interval reduced by a factor of 2 and by a factor of 4. By comparing closely the numerical results, we confirm that there are no significant differences in the results associated with the choice of time intervals. In other words, our choice of the time interval (Δt = 4.968 min.) is appropriate.

CHAPTER 7 CONCLUSION

7.1 Summary

Coastal pollution frequently results from discharges of domestic and industrial wastewater effluents. In the study, a Lagrangian random-walk model has been developed for predicting the transport of wastewater effluents discharged from a marine outfall into a tidal channel. The computations use near-field data as initial input that consists of plume trapping depth and peak concentration. It is assumed that at the end of the near-field the concentration field follows the Gaussian distribution in the vertical. The subsequent motion of effluents is predicted by solving the advection-diffusion equation.

The model is then applied to Burrard Inlet which receives wastewater discharge from the Lions Gate wastewater treatment plant. From field surveys of the discharge in the inlet, effluent concentrations, density field and flow velocities are available for input and for the validation of numerical results produced by the model. For data comparison, we match the timing and locations of the numerical results with those of the field data by identical tidal phases. Both Fickian diffusion and non-Fickian diffusion are simulated. To predict sharp variations in the concentration field as observed in the field is very challenging. In this study the model has captured quite well the variations as well as detailed features in the concentration profiles.

The above-mentioned application is just one of numerous discharge examples in coastal urbane centres. The numerical techniques from this study are robust and can potentially be used as a tool for the impact assessment of many existent and future marine outfall discharges.

7.2 Conclusion

In this study a particle-tracking model has been developed for simulations of wastewater effluent dispersion in tidal flow where the ambient water is density-stratified. The model is applied to the Lions Gate discharge in Burrard Inlet. On the basis of this application, the main findings are as follows:

a) The particle-tracking model developed in this study is shown to successfully simulate effluent dispersion in Burrard Inlet. There is a good agreement between simulated and measured effluent plumes. This represents an extension of the existent effluent dispersion methods to effluent dispersion predictions. The random walk approach is suitable for ambient conditions with time-dependent ambient flow and density stratification.

b) What is critical is to take into account the effects of density-stratification on suppressing turbulent mixing in the formulisation of the vertical diffusion coefficient. The vertical diffusion coefficient being dependent of the Richardson number appears to be adequate to parameterise the effects. The consideration of non-Fickian diffusion in the horizontal is shown to play an important role as well. The numerical results for a series non-Fickian simulations show that the spreading of effluent plumes has a non-linear dependence of the cloud size; this important aspect of the effluent dispersion in tidal waters has successfully been captured by using different values for the Hurst index.

c) A value of 0.6 for the Hurst index appears to be valid for tidal flow of moderate strength, which is within the range of 0.55 to 0.70, as reported in the literature; the values used by other investigators (e.g. 0.79 used by Osborne *et al*. and 0.75 by

Addison) appear to be too high. An increase in the Hurst index will result in spatially more uniform and dispersive effluent clouds, but will not affect the centre in the vertical of effluent plumes.

d) Should Fickian diffusion as an approximation is considered, a constant value of 0.5 m^2/s for the horizontal diffusion coefficients is appropriate. This is based on comparisons between the predicted and observed vertical structures of effluent plumes. However, using constant values for the vertical diffusion coefficient will not be able to realistically simulate effluent dispersion in density-stratified coastal waters; the vertical structure of plumes will disappear after a few tidal cycles.

e) In particle-tracking modelling the integration time interval should be as small as possible whereas the total number of particles used should be as many as possible to avoid artificial patchy plumes. In the Burrard Inlet application, the integration time interval is such that the tidal cycle is resolved by using 150 time intervals, and the discharged effluent mass is apportioned into a total of 50000 particles. These values may be used as the reference for particle dispersion modelling in coastal waters.

f) Using the model presented in this study, it is possible to identify the most desirable time windows during a tidal cycle for the disposal of waste effluents. Comparisons among various scenarios of the predicted movement of particle clouds may lead to the choice of the shortest residence time of waste effluents in the receiving water. For example, in the Burrard Inlet case, it is not surprising that the best scenario is to discharge effluents in time periods of ebbing tides; within 5 hours following the

release of effluents, 85% of the particles (effluents) flow out of the channel in the direction of ebbing flow.

7.3 Future Research

The main limitations of the present study are associated with the availability of input and validation data. Nevertheless, the present study may be extended to include:

a) the effects of particle settling velocity, which would be important for the study of the long-term impacts of wastewater discharges on the receiving water bodies;

b) ambient flow and density fields in fully three dimensions. It is feasible to obtain a good description of three-dimensional flow and density fields from separate or coupled hydrodynamics calculations;

c) the direct interaction between the near-field and far-field. With this interaction, modelling tools will be of full prediction capacity;

d) a practical assessment of the impacts of different discharge options, including the current and future conditions of effluent discharge.

REFERENCES

Addison, P. S., Qu, B., Nisbet, A. and Pender, G. 1997. A non-Fickian particle-tracking diffusion model based on fractional Brownian motion. *International journal for numerical methods in fluids* **25**: 1373–1384.

Albertson, M. L., Dai, Y. B., Jensen, R. A., Rouse, H. 1950. Diffusion of submerged jets. *Trans. ASCE* **115**: 639–97.

Banton, O., Delay, F. and Porel, G. 1997 A new time domain random walk method for solute transport in 1-D heterogeneous media. *Ground Water* **35**: 1008–1013.

Barry, D. A. 1990. Supercomputers and their use in modelling subsurface solute transport. *Rev. of Geophysice* **28**(3): 277–295.

Bensabat, J., Zhou, Q. and Bea, J. 2000. An adaptive pathline-based particle tracking algorithm for the Eulerian-Lagrangian method. *Advances in Water Resources* **23**: 383–397.

Brooks, N.H. 1956. Methods of analysis of the performance of ocean outfall diffusers with application to the proposed Hyperion outfall. *Report to Hyperion Engineers, Los Angeles, Calif.* pp. 36.

Brooks, N.H. 1960. Diffusion of sewage effluent in an ocean current. Proceedings of the 1st International Conference on Waste Disposal in the Marine Environment, Pergamon Press, New York, pp. 246–267.

Brooks, N. H., Koh, R. C. Y. 1965. Discharge of sewage effluent from a line source into a stratified ocean. *Water Quality Control Plan for Ocean Waters of California*. July 6, 1972. pp. 15.

Cederwall, K. 1975. Gross parameter solutions of jets and plumes. *Journal of Hydraulic Engineering, ASCE* **101**: 489–509.

Chin, D. A. Chin and Roberts, P. J. W. 1985. Model of dispersion in coastal waters. *Journal of Hydraulic Engineering, ASCE* **111**: 12–28.

Fan, L. N., Brooks, N. H. 1969. Numerical solutions of turbulent buoyant jet problems. *Calif Inst. Technol., W. M. Keck Lab. Rep*. No. KH-R–18.

Fox, R. O., Liu, Y., Raman, V. 2004. Scale up of gas-phase chlorination reactors using CFD. *Chemical Engineering Science* **59:** 5167–5176.

Godin, G. 1972. The Analysis of Tides, University of Toronto Press, Toronto, pp.264.

Hathhorn, W. E. 1997. Simplified approach to particle tracking methods for contaminant transport. *Journal of Hydraulic Engineering, ASCE* **123**: 1157–1160.

Hurst, H. E. 1951. Long term storage capacity of reservoirs. *Trans. ASCE* **116**: 770–808.

Hurst, H. E. 1956. Method of using long-term storage in reservoirs. Proc. Inst. *Journal of Civil engineering* **5**: 519–577.

James, G. 2004. Advanced modern engineering mathematics. *Third Edition,* Prentice-Hall, Harlow, England, pp. 950.

Jeng, S. W., and Holley, E. R. 1986. Two-dimensional random walk model for pollutant transport in natural rivers. Center for Research in Water Resources, Univ. of Texas, Austin, Texas.

Jirka, G. H. and Doneker, R. L. 1991. Hydrodynamic classification of submerged single-port discharges. *Journal of hydraulic engineering ASCE* **117**: 1095–1112.

Jirka, G. H. and Akar, P.J. 1991. Hydrodynamic classification of submerged multiport-diffuser discharges. *Journal of Hydraulic Engineering ASCE* **117**: 1113–1128.

Kay, A. 1987. The effect of cross-stream depth variations upon contaminant dispersion in a vertically well-mixed current. *Estuarine, Coast and Shelf Science* **24**: 177–204.

Kim, Y. D. and Seo, I. W. 2001. Modeling the mixing of wastewater effluent discharged from ocean outfall using hybrid model. *Coastal Engineering Journal* **43**: 259–288.

Kinzelbach, W. 1986. Groundwater modelling: an introduction with sample programs in basic. Elsevier, New York, pp. 298–315.

Kinzelbach, W. 1988. The random walk method in pollutant transport simulation. *Groundwater Flow and Quality Modeling,* pp. 227–246.

Kinzelbach, W. and Uffink, G. 1991. The random walk method and extensions in groundwater modelling. in Bear, J. and Corapacioglu, M. Y. Eds, Transport Processes in Porous Media. *Kluwer Academic, Hingham, MA*, pp. 761–787.

Koh, R. C. Y. and Brookes, N. H. 1975. Fluid mechanics of waste-water disposal in the ocean. *Annual Review of Fluid Mechanics* **7**: 187–211.

Lee, J. H. W. and Chu, V. H. 2003. Turbulent Jets and Plumes: A Lagrangian Approach. *Kluwer Academic Publishers*, Norwell, Massachusetts.

Li, S. S. and Hodgins, D.O. (2004) A dynamically coupled outfall plume-circulation model for effluent dispersion in Burrard Inlet, British Columbia. *Journal of Environmental Engineering and Science* 3**:** 433–449.

Li, S. S. and Hodgins, D. O. 2010. Modeling wastewater effluent mixing and dispersion in tidal channel. *Canadian Journal of Civil Engineering* **3**1(1): 99–111.

List, E. J., Gartrell, G. and Winant, C. D. 1990 Diffusion and dispersion in coastal waters. *Journal of Hydraulic Engineering* **116**: 1158–1179.

Luhar, A. K. and Britter, R. E.: 1989, A random walk model for dispersion in inhomogeneous turbulence in a convective boundary layer. *Atmospheric Environment* 23(7): 1911–1924.

Luhar and Sawford, 1995. A.K. Luhar and B.L. Sawford, Lagrangian stochastic modelling of the coastal fumigation phenomenon. *J. Appl. Met.* **34**: 2259–2277.

Morton, B. R., Taylor, G. I., Turner, J. S. 1956. Turbulent gravitational convection from maintained and instantaneous sources. *Proc. Roy. London Ser.* A **234**: 1–23.

Osborne, A. R., Kirwan, A. D. Provenzale, A. and Bergamasco, L. 1989. Fractal drifter trajectories in the Kuroshio extension. *Tellus,* **41A:** 416–35.

Pearce, B. R., and others 1990. Thermal plume study in the delaware river: prototype measurements and numerical simulation. IAHR International Conference on Physical Modeling of Transport and Dispersion, 13B.7-13B.12, Cambridge, Mass.

Prickett, T. A., T. G. Naymik, and C. G. Lonnquist. 1981. A random walk solute transport model for selected groundwater quality evaluations. *Illinois State Water Survey*. Bulletin pp. 65–103.

Rawn, A. M., and Palmer, H. K. 1930 Pre-determining the extent of sewage field in sea water. *ASCE Trans.* **94**: 1037–1071.

Rawn, A. M., Bowerman, F. R., Brooks, N. H. 1961. Diffusers for disposal of sewage in sea water. *Trans. ASCE* **126**: Part III, 344-388.

Rouse, H., Yih, C. S., Humphreys, H. W. 1952 Gravitational convection from a boundary source. *Tellus* **4**: 201–10.

Roberts, P. J. W., Snyder, W. H. and Baumgartner, D. J. 1989a. Ocean outfalls. I: submerged wastefield formation. *Journal of Hydraulic Engineering, ASCE* **115**(1): 1– 25.

Roberts, P. J. W., Snyder, W. H. and Baumgartner, D. J. 1989b. Ocean outfalls II: spatial evolution of submerged wastefield. *Journal of Hydraulic Engineering, ASCE* **115**(1): 26–48.

Roberts, P. J. W., Snyder, W. H. and Baumgartner, D. J. 1989. Ocean outfalls III: effect of diffuser design on submerged wastefield. *Journal of Hydraulic Engineering, ASCE* **115**(1): 49–70.

Sanderson, B. G. and Booth, D. A. 1991. The fractal dimension of drifter trajectories and estimates of horizontal eddy-diffusivity. *Tellus* **43A**: 334–349.

Scheidegger, A. E. 1954. Statistical hydrodynamics in porous media. *Applied Physics* **25**(8): 145–58.

Scott, C.F. 1997. Particle Tracking Simulation of Pollutant Discharges. *Journal of Environmental Engineering, ASCE* **123**: 919-927.

Seaconsult and EVS. (1999). Fate and effects of discharges from the Lions Gate Wastewater Treatment Plant. Greater Vancouver Regional District. Vancouver, B.C.

Socolofsky, S.A. and Jirka, G.H. 2005. Special topics in mixing and transport processes in the environment. Coastal and Ocean Engineering Division, Texas A&M University pp. 1–39.

Stevens, C.L., Lawrence, G.A., and Hamblin, P.F. 2004. Horizontal dispersion in the surface layer of a long narrow lake. *Journal of Environmental Engineering Science* **3**: 413–417.

Tajima, Y., Kozuka, M., Tsuru, M. Ishii, T. Sakagami, T. Momose, K. Mimura, N. and Madsen, O. S. 2007. Model of dispersion in coastal waters. *Journal of Hydraulic Engineering, ASCE* Coastal Sediments **7**: 1–14.

Thomson, R.E. 1981. Oceanography of the British Columbia Coast. Can. Spec. Publ. Fish Aqut. Sci. **56** pp. 45–61 and pp. 139–179.

Valocchi, A. J. And Quinodoz, A. M. 1989 Application of the random walk method to simulate the transport of kinetically adsorbing solutes. *Groundwater Contamination* (proceedings of the symposium held during the Third IAHS Scientific Assembly, Baltimore, MD, May 1989) pp. 35–42.